Contrib Mineral Petrol (2015) 170:54
DOI 10.1007/s00410-015-1207-7

ORIGINAL PAPER

The magma plumbing system for the 1971 Teneguía eruption on La Palma, Canary Islands

Abigail K. Barker[1] · Valentin R. Troll[1,2] · Juan Carlos Carracedo[2] · Peter A. Nicholls[1]

Received: 1 June 2015 / Accepted: 11 November 2015 / Published online: 26 November 2015

Abstract The 1971 Teneguía eruption is the most recent volcanic event of the Cumbre Vieja rift zone on La Palma. The eruption produced basanite lavas that host xenoliths, which we investigate to provide insight into the processes of differentiation, assimilation and magma storage beneath La Palma. We compare our results to the older volcano magmatic systems of the island with the aim to reconstruct the temporal development of the magma plumbing system beneath La Palma. The 1971 lavas are clinopyroxene-olivine-phyric basanites that contain augite, sodic-augite and aluminium augite. Kaersutite cumulate xenoliths host olivine, clinopyroxene including sodic-diopside, and calcic-amphibole, whereas an analysed leucogabbro xenolith hosts plagioclase, sodic-augite-diopside, calcic-amphibole and hauyne. Mineral thermobarometry and mineral-melt thermobarometry indicate that clinopyroxene and plagioclase in the 1971 Teneguía lavas crystallised at 20–45 km depth, coinciding with clinopyroxene and calcic-amphibole crystallisation in the kaersutite cumulate xenoliths at 25–45 km and clinopyroxene, calcic-amphibole and plagioclase crystallisation in the leucogabbro xenolith at 30–50 km. Combined mineral chemistry and thermobarometry suggest that the magmas had already crystallised, differentiated and formed multiple crystal populations in the oceanic lithospheric mantle. Notably, the magmas that supplied the 1949 and 1971 events appear to have crystallised deeper than the earlier Cumbre Vieja magmas, which suggests progressive underplating beneath the Cumbre Vieja rift zone. In addition, the lavas and xenoliths of the 1971 event crystallised at a common depth, indicating a reused plumbing system and progressive recycling of Ocean Island plutonic complexes during subsequent magmatic activity.

Keywords Mineral chemistry · Thermobarometry · Magma plumbing · La Palma · Canary Islands

Introduction

La Palma and the neighbouring island of El Hierro are the westernmost islands of the Canary archipelago (Fig. 1). Both islands are active volcanoes with the last eruption observed at El Hierro in 2011 and frequent historic eruptions documented on La Palma over the last centuries (Carracedo et al. 2001, 2012; Klügel et al. 1999, 2005, Troll et al. 2012). The most recent eruption on La Palma occurred in 1971 and is known as the Teneguía eruption, after a local aboriginal place name. The 1971 Teneguía eruption is relevant in a regional context as it provides a link between the current magma plumbing system and the systems that supplied the preceding 1949 and earlier eruptions, thus allowing us to trace the temporal development of the magma plumbing system beneath La Palma. However, the 1971 Teneguía eruption has had comparatively little attention by the international scientific community and therefore we present a detailed account of the eruption and its products. Our investigation of the relationship between

Communicated by Jochen Hoefs.

Electronic supplementary material The online version of this article (doi:10.1007/s00410-015-1207-7) contains supplementary material, which is available to authorized users.

✉ Abigail K. Barker
abigail.barker@geo.uu.se

[1] CEMPEG, Department of Earth Sciences, Uppsala University, Uppsala, Sweden

[2] GEOVOL, Universidad de Las Palmas, 35017 La Palmas Gran Canaria, Spain

magmatic processes and eruptive behaviour will likely help to provide an improved basis for informed hazard assessment at La Palma and El Hierro during future eruptive events (cf. Carracedo et al. 2015).

We specifically present mineral and whole-rock compositional data and employ single-mineral and mineral-melt thermobarometry for the 1971 Teneguía lavas and their xenoliths, to determine the depth of mineral formation and assess the relationships between the magma and associated xenoliths. Using the combined findings, we propose a model for the lithospheric architecture and magmatic processes beneath La Palma.

Geological history of La Palma

Volcanic activity at La Palma commenced with the formation of a submarine complex of seamounts and associated plutonics between 3 and 4 Ma (Staudigel et al. 1986; Carracedo et al. 1999). The submarine evolution of La Palma was followed by the old volcanic series, associated with the Garafia and Taburiente shield volcanoes and the Cumbre Nueva rift zone, which is part of the Taburiente suite (850–560 kyear; Carracedo et al. 2001). The younger Bejenado complex grew in the southwest-oriented landslide scar of the Taburiente volcano (Fig. 1; Carracedo et al. 1999, 2011). Following the decline of activity at the Taburiente and Bejenado volcanoes, the volcanism propagated southwards to form the Cumbre Vieja rift zone from ca. 125 ka onwards, which hosts the presently active volcanic system on La Palma (Fig. 1; Carracedo et al. 1999, 2001).

Eruptive history of the Cumbre Vieja rift zone

La Palma is historically the most active of the Canary Islands with relatively frequent eruptions from the Cumbre Vieja rift zone, that include the 1585, 1646, 1677, 1712, 1949 events and the last eruption of 1971 from the Teneguía volcano (Carracedo et al. 2001). The Cumbre Vieja rift zone eruptions commenced with pre-historic events dating back some 125 ka (Carracedo et al. 2001). Characteristics of the historic eruptions from the Cumbre Vieja rift zone include the connection to phonolitic domes (Day et al. 1999), probably due to new magma exploiting the intense fracture systems associated with the domes that act as easy pathways (e.g. *Roque Teneguía* in the case of the 1971 event). Another common feature is the eruption from multiple vents, generally aligned along several kilometre long fissures, usually parallel but occasionally oblique to the rift axis (Klügel et al. 2000; Day et al. 2000; Carracedo et al. 2001). Notably, the higher-altitude vents are predominantly characterised by explosive phreatic eruptions (gas-rich), whereas the lower-altitude vents usually produce larger scoria deposits and lava flows.

Fig. 1 **a** A photograph from northern La Palma featuring the Taburiente volcano in the foreground, the Bejenado volcano in the middle and the Cumbre Vieja rift zone in the distance. **b** Geological map of La Palma that shows the main volcanic centres with the pre-historic to historic eruptions of the Cumbre Vieja rift zone, the most recent eruptions are labelled (modified after Carracedo et al. 1999, 2001 and Klügel et al. 2005)

The historic eruptions of the Cumbre Vieja rift, including the 1971 Teneguía eruption, produced basanitic to phonolitic lavas and associated scoria deposits (Carracedo et al. 1999; Klügel 1998; Klügel et al. 1997, 2000, 2005). The geological map shows the distribution of the historic eruption products along the Cumbre Vieja rift zone (Fig. 1). Most of the historic eruptions, such as those in 1585, 1646, 1712 and 1949 events, were emitted from vents on the crest of the rift zone, whereas the 1677 and 1971 events were erupted from the southern tip of the island. The products of the historic eruptions are typically zoned (Hernandez-Pacheco and Valls 1982; Klügel et al. 1999) and contain a spectrum of xenoliths, including peridotites, tholeiitic gabbro, kaersutite-bearing assemblages, alkali gabbro, leucogabbro, syenite as well as exotic quartz-bearing xenopumice (Araña and Ibarrola 1973; Muñoz et al. 1974; Neumann et al. 2000; Klügel et al. 1999, 2000, 2005a, b).

The 1971 Teneguía eruption

The Teneguía eruption (Figs. 1, 2) is the most recent eruption on La Palma, and it occurred near a phonolite dome (*Roque de Teneguía*). The 1971 eruption vents are located close to the town of *Fuencaliente* and near the 1677 eruptive vents. The 1971 eruption was characterised by strombolian eruptive behaviour, emitting tephra and lava from a group of volcanic vents, between 26 October and 18 November 1971 (Fig. 2; Afonso et al. 1974; Araña and Fúster 1974). The lavas reached the sea and formed a coastal lava platform, albeit of limited dimensions. The eruption was preceded by strong seismicity, focused in the area where the eruption eventually took place. It began by opening a several-hundred-metre-long fissure in the afternoon of 26 October, which gave rise to the first lava flows, that quickly descended towards the coast southeast and southwest of the vents (Fig. 2). Following several weeks of strombolian activity and emission of lava, the eruption ceased rather abruptly on 18 November.

The 1971 Teneguía eruption displayed two main phases. The first phase was characterised by the formation of two eruptive centres (No. l and 2; Fig. 2b), aligned along a >300-m-long fissure and dominated by lava effusion throughout the duration of the eruption (Afonso et al.

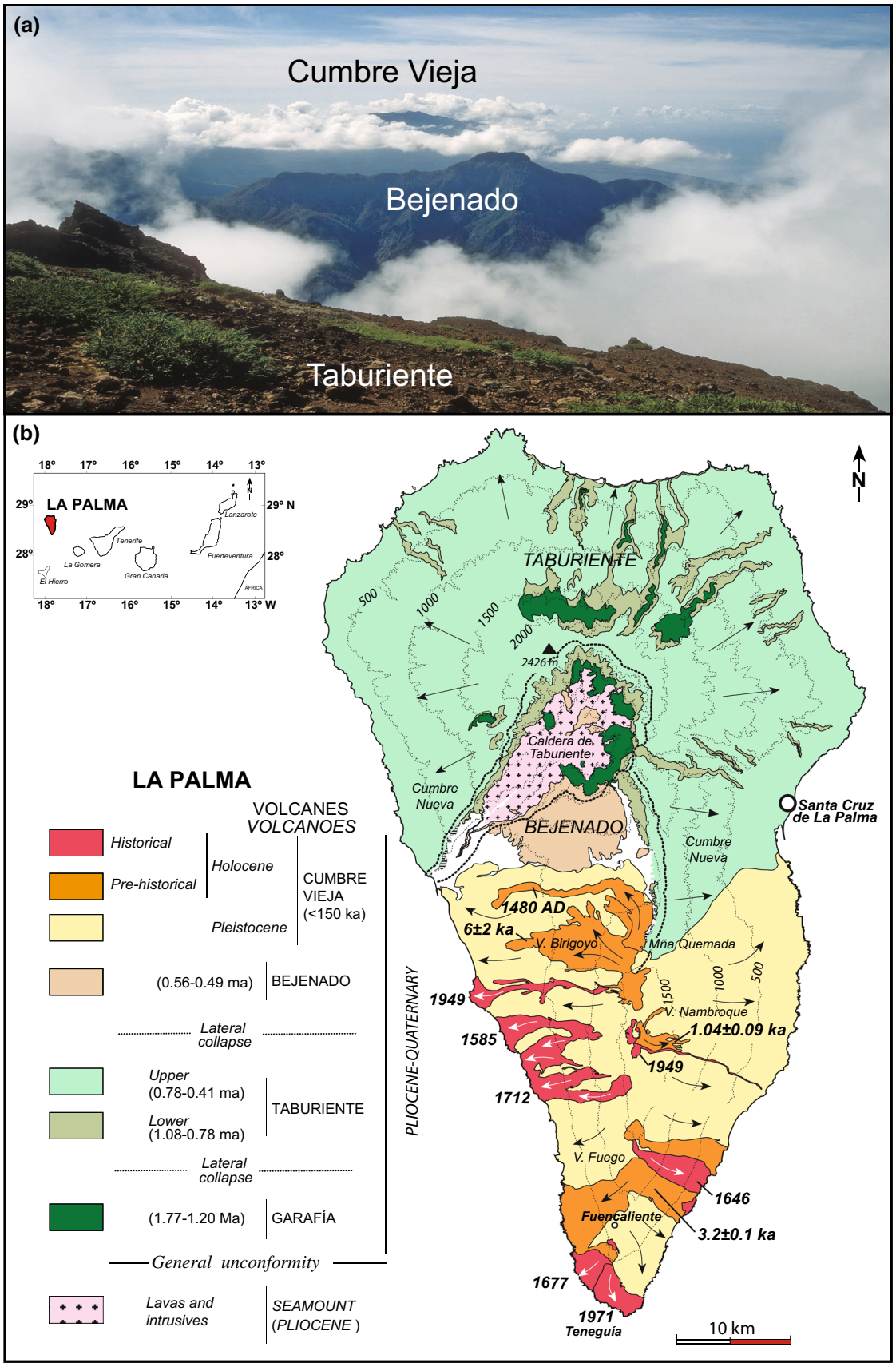
(a)
Cumbre Vieja
Bejenado
Taburiente
(b)
LA PALMA
Lanzarote
Tenerife
Fuerteventura
La Gomera
Gran Canaria
El Hierro
AFRICA
TABURIENTE
BEJENADO
Caldera de Taburiente
Cumbre Nueva
Santa Cruz de La Palma
2426m
1480 AD
6±2 ka
V. Birigoyo
Mña Quemada
1949
1585
1712
V. Nambroque
1.04±0.09 ka
1949
V. Fuego
1646
Fuencaliente
3.2±0.1 ka
1677
1971
Teneguía
10 km
PLIOCENE-QUATERNARY
LA PALMA
VOLCANES
VOLCANOES
Historical
Pre-historical
Holocene
Pleistocene
CUMBRE VIEJA (<150 ka)
(0.56-0.49 ma)
BEJENADO
Lateral collapse
Upper (0.78-0.41 ma)
Lower (1.08-0.78 ma)
TABURIENTE
Lateral collapse
(1.77-1.20 Ma)
GARAFÍA
General unconformity
Lavas and intrusives
SEAMOUNT (PLIOCENE)

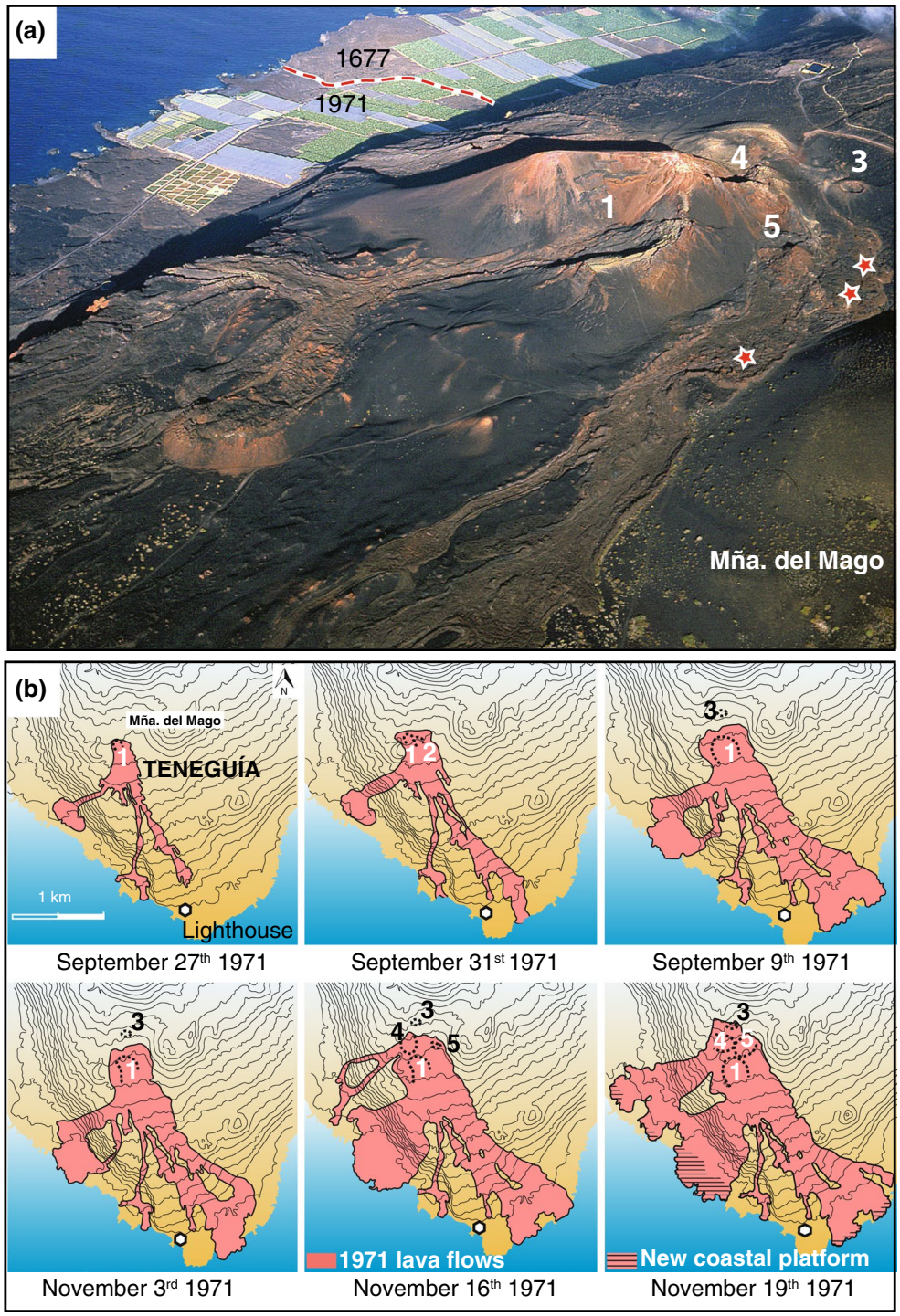

Fig. 2 Location of volcanic vents and products of the 1971 Teneguía eruption. **a** Distribution of the vents associated with the 1971 Teneguía eruption; **b** evolution of vents and lava flows in 1971 (after Afonso et al. 1974; Carracedo et al. 2001). Note that vent 2 was covered during the eruptive activity of vents 4 and 5. Samples for this study were collected from the lava flow to the east of the vent complex (marked by *red stars*)

1974). The second phase was characterised by the formation of several new eruptive vents starting on 8 November, that likewise emitted lava flows, apart from one exception (No. 3, Fig. 2b), which was characterised by intense gas emission, but an absence of lava production. Vent 2 was destroyed by volcanic activity during this second phase and is no longer exposed (Afonso et al. 1974; Araña and Fúster 1974).

The two phases of the eruption display differences in petrography and composition. The first phase was composed of amphibole-bearing pyroxene basanites with MgO contents of 6.7–7.8 wt%, whereas the second phase showed less amphibole and the resulting pyroxene-olivine-basanites have higher MgO content of 8.4–10.2 wt% (Fernández Santín et al. 1974; Ibarrola 1974). The samples described in this study were collected from the main lavas to the east of the vent complex (Fig. 2; Afonso et al. 1974). Thus, the samples are derived from the later products of the eruption and belong to the second phase of the eruption (Fernández Santín et al. 1974).

The Teneguía eruption was furthermore characterised by rhythmic explosions that produced fine lapilli and coarse scoria as well as some larger lava bombs in the vicinity of the vents (Afonso et al. 1974). Gases liberated during the 1971 eruption were mainly carbon monoxide (CO) and carbon dioxide (CO_2) (Chaigneau 1974). Carbon dioxide was much more abundant than carbon monoxide, and both are heavier than air and therefore prone to accumulate in depressions. Volcanic gases were most likely the reason for the two fatalities associated with the 1971 eruption, causing the asphyxiation of a fisherman working in the proximity of the lighthouse and a photographer taking pictures of the lava flows near the coast.

Although the 1971 eruption covered an existing land area of 135,000 m^2, it also produced a 290,000 m^2 lava platform and thus new land was created. The total volume of emitted materials is estimated to be ca. 40×10^6 m^3. The cumulative thickness of the lava flows is estimated to be some 12 m, while the main vents reached a height of around 100 m above the pre-eruptive land surface (Fig. 2).

Previous research on magma storage at La Palma

Previous thermobarometry studies have focused on clinopyroxene and fluid inclusions in the older lavas from La Palma (Klügel et al. 1997, 1999, 2000, 2005; Galipp et al. 2006). The magmas supplying the pre-historic eruptions of the Taburiente, Cumbre Nueva and Bejenado complexes of La Palma have been shown to have pooled and differentiated at 16–40 km depth, i.e. in the oceanic lithosphere. In contrast, the magmas that fed the younger Cumbre Vieja eruptions are reported to have crystallised from shallower magma pockets at 15–26 km depth (Galipp et al. 2006). The changes in crystallisation depths are associated with a lateral switch in magmatic activity from the older northern volcanic centres to the Cumbre Vieja rift zone, which led Galipp et al. (2006) to propose that the Cumbre Vieja rift zone is fed by a distinct magmatic system from that of the older volcanoes on the north of the island. Furthermore, clinopyroxene phenocrysts in the 1949 lavas have been stored at 15–26 km and possibly up to 36 km (Klügel et al. 2000), while fluid inclusions hosted by these clinopyroxene crystals reveal shallow crustal storage at 7–14 km depth (Klügel et al. 2000).

A wide variety of xenoliths assemblages have been recovered from the 1949 and 1971 lavas including kaersutite-bearing assemblages, alkali gabbro, leucograbbro, syenite, tholeiitic gabbro, peridotite and quartz-bearing assemblages, and similar xenoliths have also been described from some of the older historic and pre-historic Cumbre Vieja eruptions (Araña and Ibarrola 1973; Muñoz et al. 1974; Klügel et al. 1997, 2000; Klügel 1998; Carracedo et al. 1999, 2001; Neumann et al. 2000). The peridotite xenoliths often grow rims or selvages in the host magma on passage through the lithosphere that indicate residence times on the order of several years, and additional density data from fluid inclusions in these selvages place the equilibration at crustal depths (Klügel et al. 1997; Klügel 1998).

Analytical methods

Mineral chemistry of the olivine in the lavas and the kaersutite cumulate xenoliths was analysed by a Cameca SX50 electron microprobe at Uppsala University using run conditions of 20 kV and 15 nA. Calibration and standardisation were based on international reference materials. Typical reproducibility is reported as a function of element concentration, oxides with >10 wt% at ± 1–5 %; oxides with 1–10 wt% at ± 5–10 %; oxides with <1 wt% at ± 10 % (Andersson 1997). The newer JEOL JXA-8530F HyperProbe at CEMPEG, Uppsala University, was used to analyse all other mineral phases such as clinopyroxene, amphibole and plagioclase in the lavas and xenolith samples. The operating conditions for the JEOL JXA-8530F HyperProbe were 15 kV and 10 nA, and the Phi Rho Z (PRZ) correction was automatically applied to the raw data. Elemental maps were analysed with the JEOL JXA-8530F Hyperprobe using the wavelength-dispersive system (WDS) with 100 s dwell times at 10 nA and 15 kV. Analytical precision was measured on Smithsonian Institute mineral standards, which show that oxides with concentrations of >10 wt% give uncertainties of ≤1.5 % s.d., and oxides with concentrations of 5–10 wt% give uncertainties of ≤2.2 % s.d., with oxides at lower concentrations having analytical uncertainties of ≤10 % s.d. (see supplementary methods for further details).

Whole-rock geochemistry was performed on the lavas and kaersutite cumulate xenoliths; however, the leucogabbro xenolith was not analysed for whole-rock geochemistry as the sample was too small to provide sufficient material for analysis. The samples were prepared by jaw crushing

and milling. The samples (0.5 g) were digested with a $LiBO_2/Li_2B_4O_7$ flux for major element analysis by inductively coupled plasma emission spectrometry (ICP-ES) at ACME Analytical Laboratories Ltd in Vancouver, Canada. The trace elements analyses were prepared by digestion of 0.25 g of sample material in HNO_3–$HClO_4$–HF and analysed by inductively coupled plasma mass spectrometry (ICP-MS) at ACME Analytical Laboratories Ltd in Vancouver, Canada. Internal standards and duplicates record analytical precision, where for the major elements with contents of >2 wt% the reproducibility is $\leq\pm0.5$ %, and for the major element with contents of <2 wt% the reproducibility reaches up to ±1.2 wt%, likewise for trace elements with concentrations >10 ppm the reproducibility is $\leq\pm11$ %, whereas at concentrations of <10 ppm the reproducibility is on the order of $\leq\pm0.6$ ppm.

Results

Petrography

We present lava samples from the second phase of the 1971 Teneguía eruption ($n = 10$), which are highly vesicular porphyritic clinopyroxene-olivine-basanites (Fernández Santín et al. 1974). There are multiple populations of clinopyroxene phenocrysts (10–15 %; 100 to >1000 μm) ranging from colourless or light brown to green, with euhedral to anhedral shapes that are frequently fractured (Fig. 3a, b). Clinopyroxene is typically homogeneous with a small proportion of samples showing a large homogeneous core surrounded by a single rim (Fig. 3e, f; Brändle et al. 1974; Prægel 1986). Olivine makes up 5–10 % (100 to >1000 μm) of the lava samples, and minor small phenocrysts of plagioclase are found (ca. 100 μm) in a clinopyroxene and plagioclase microlitic groundmass. Additionally, glomerocrysts containing clinopyroxene, plagioclase, amphibole, titanite, apatite and iron oxides in varying proportions are observed (Fig. 3c). The lavas also host xenocrysts that are commonly rounded and tend to be rich in inclusions. The xenocrysts are often amphibole, which is also the likely origin for amphibole in the first phase of the eruption (<4000 μm; Fig. 3d; Fernández Santín et al. 1974), but xenocrysts of albite, aegirine-augite, titanite and apatite also occur.

The lavas of the 1971 Teneguía eruption also entrained several types of xenoliths. The most proliferous were amphibole-bearing xenoliths, which represent ca. 55 % of the total observed xenolith suite and became more abundant during the eruption accounting for up to ca. 66 % in the second phase of the eruption (Muñoz et al. 1974). We have sampled five amphibole-bearing xenoliths, and following Muñoz et al. (1974), we distinguish two lithological groups on the basis of mineralogy, petrography and geochemistry. However, previous studies of xenoliths at La Palma have not come to a consensus for nomenclature of these amphibole-bearing xenoliths. The most common type of xenoliths is mafic to ultramafic plutonics up to 10 cm in length, and they are typically rounded and display sharp contacts with the vesicular lava (Fig. 4c). These xenoliths have been referred to as amphibole-bearing xenoliths (Muñoz et al. 1974), hornblendites (Neumann et al. 2000) and kaersutitites (Klügel et al. 1999, 2000). We follow the latest IUGS nomenclature and use the name kaersutite cumulates (Le Maitre et al. 2002). Occasionally evolved plutonic xenoliths a few centimetres in length are also found in the 1971 Teneguía lavas (Fig. 4a), which have previously been described as amphibole-plagioclase-bearing xenoliths (Muñoz et al. 1974), leucograbbro to syenite (Neumann et al. 2000) and alkali gabbro (Klügel et al. 1999). Their alkaline character is confirmed by the presence of the distinctive blue mineral hauyne, and we adopt the terminology leucogabbro for these xenoliths on the basis of their light-coloured appearance and relatively evolved character.

One xenolith sample is a leucogabbro that has a poikilitic texture and is composed of feldspar (≤1000 μm; 50–70 %), calcic-amphibole (10–15 %), mostly green pyroxene (10–20 %) and accessory hauyne, titanite and apatite (Fig. 4b). The majority of the xenolith samples are kaersutite cumulates ($n = 4$). The kaersutite cumulate xenoliths contain colourless clinopyroxene (10–60 %), calcic-amphibole (10–40 %), green pyroxene (0–40 %), olivine, phlogopite and Fe–Ti-oxides (Fig. 4d), and amphibole is observed to be an interstitial to poikilitic phase. The minerals have grain sizes of 1000 to >4000 μm with interstitial phases of <100 μm. Inclusions are abundant in the minerals of the kaersutite cumulate xenoliths, commonly occurring in clinopyroxene but also in calcic-amphibole. They vary from single-phase inclusions to two- and three-phase inclusions. The majority of the inclusions are fluid inclusions, but melt inclusions also occur. The fluid and melt inclusions range in size from a few μm to 50 μm in diameter (Fig. 4e, f). The fluid inclusions can be classified as primary that formed as the minerals grew (ca. 40 %) or secondary that formed after mineral growth (ca. 60 %). The secondary fluid inclusions form along fractures, grain boundaries or cleavage planes and as trails of very small inclusions. Pseudo-secondary fluid inclusions occur in healed fractures. Spheroidal to elongated shapes suggest stretching during deformation of the host phenocrysts. Double inclusions and inclusions with haloes or wings indicate the occurrence of decrepitation (cf. Sterner and Bodnar 1989; Bakker and Jansen 1994; Vityk and Bodnar 1995; Van der Kerkoff and Hein 2000).

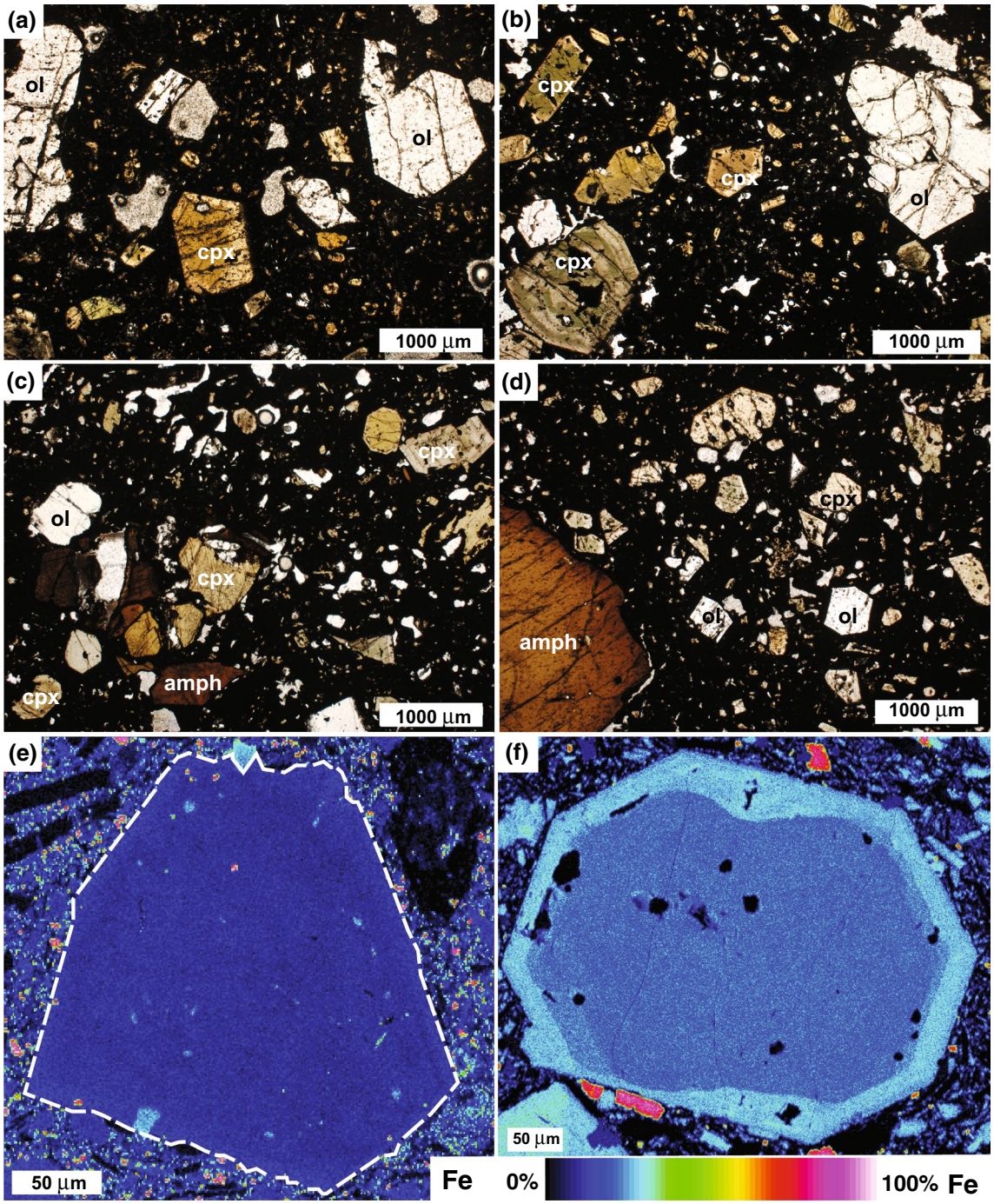

Fig. 3 Representative photomicrographs of the 1971 Teneguía lavas; **a** clinopyroxene- and olivine-bearing basanite, **b** *green*, *colourless* and *brown* pyroxene phenocrysts are present with olivine in a microcrystalline groundmass, **c** glomerocryst of xenocrystic calcic-amphibole and clinopyroxene in a vesicular clinopyroxene- and olivine-bearing basanite, **d** Phenocrysts of clinopyroxene and olivine together with a large xenocryst of calcic-amphibole. Elemental maps of iron for clinopyroxene **e** the most common type of clinopyroxene is unzoned, and **f** a small proportion of clinopyroxene phenocrysts in five of the lava samples show this typical simple core and rim zonation. *ol* olivine, *cpx* clinopyroxene, *amph* calcic-amphibole

Mineral chemistry

The lavas host olivine with Fo content of 66–86 % and an average Fo content of 80.7 ± 4.6 % and CaO of 0.20 ± 0.09 wt% (2s.d.; $n = 239$; Fig. 5a). The clinopyroxene in the lavas can dominantly be classified as augite that extends into the diopside field ($Wo_{42–47}En_{42–51}Fs_{16–27}$); they show a range in Mg# of 54–83 and mean Mg# of

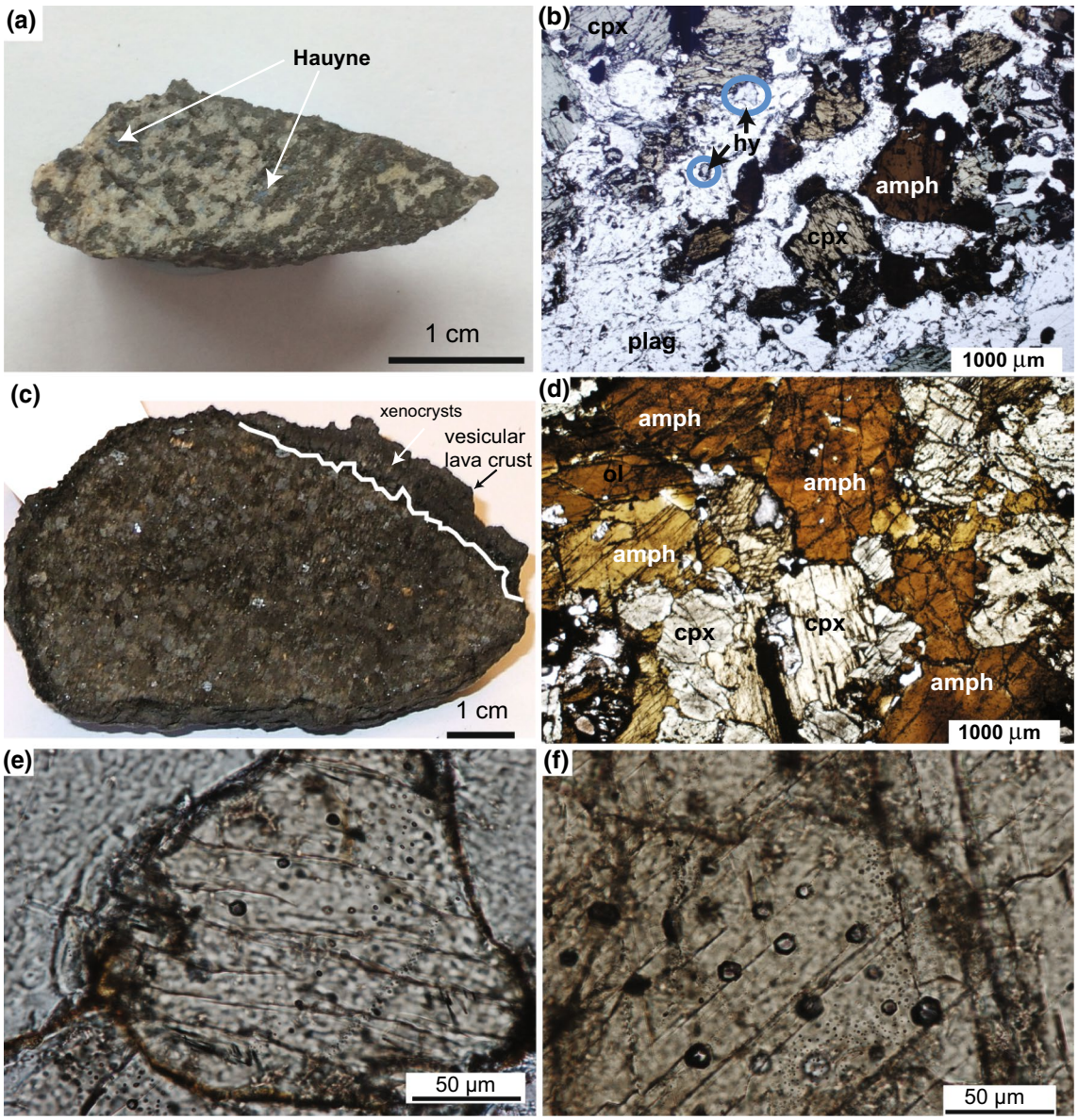

Fig. 4 Plutonic xenoliths sampled by the 1971 Teneguía eruption; **a** photograph of a hand specimen of a hauyne-bearing leucogabbro xenolith, **b** photomicrograph of the leucogabbro xenolith, showing calcic-amphibole, *green* pyroxene, plagioclase and hauyne. **c** Photograph of a hand specimen of an kaersutite cumulate xenolith with a crust of vesicular basanite, notice that occasional crystals from the alkali gabbro are mingling into the basanite, **d** photomicrograph of an kaersutite cumulate xenolith that features calcic-amphibole and clinopyroxene, **e** photomicrograph of primary fluid inclusions in clinopyroxene showing two phases: vapour and liquid or liquid and solid, and **f** photomicrograph of secondary fluid inclusions associated with clinopyroxene cleavage, showing single- and two-phase varieties. *cpx* clinopyroxene, *amph* calcic-amphibole, *plag* plagioclase, *hy* hauyne (*circled*)

72.7 ± 10.2 (2s.d.; $n = 574$ in 557 crystals; Figs. 5b, 6). Most of the clinopyroxene phenocrysts are homogeneous, but those with two zones have cores that range in colour from beige to green and have Mg# of 57–78, whereas the corresponding rims have Mg# of 67–79 (Fig. 7a; $n = 17$ zoned crystals; Brändle et al. 1974). The rims generally have higher Mg# than the cores, suggesting processes of magma recharge and mixing occurred. The clinopyroxene phenocrysts display a wide range of compositions that reflect multiple populations, and overall positive correlations between FeO (5.5–13.1 wt%) and Na_2O (0.3–1.7 wt%) as well as between Al_2O_3 (1.0–11.1 wt%) and TiO_2 are observed (0.14–5.50 wt%) (Fig. 7). The different populations of pyroxene are represented by high sodium content and green colour of sodic-augite and elevated Al content of aluminium augite (Brändle et al. 1974). These types of clinopyroxene are found in all samples and are consistent with the previous observation of multiple

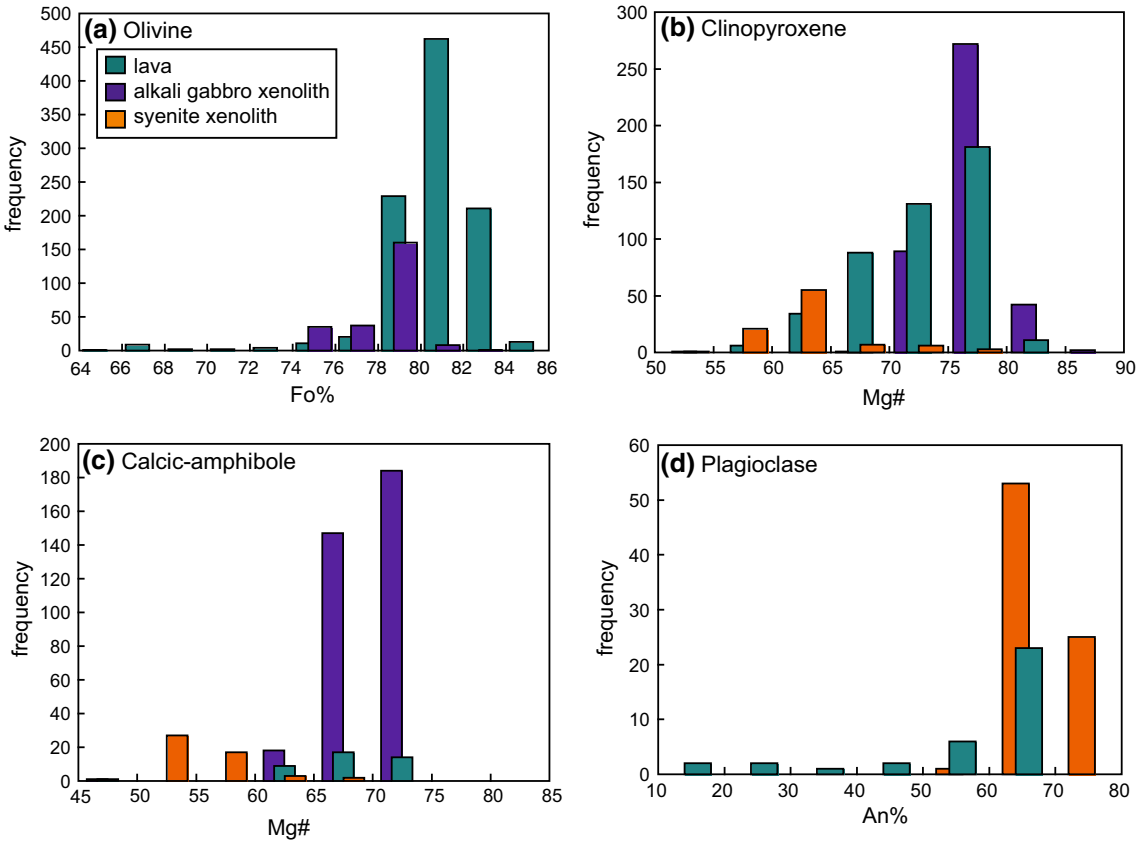

Fig. 5 Mineral chemistry of the main phases found in the 1971 Teneguía lavas, kaersutite cumulate xenoliths and leucogabbro xenolith; **a** Fo content of olivine, **b** Mg# of clinopyroxene, **c** Mg# of calcic-amphibole and **d** a content of plagioclase

populations of pyroxene in the two phases of the eruption Prægel (1986). Plagioclase shows a range in An content from 12 to 67 % ($n = 36$), extending from labradorite to xenocrysts of oligoclase (Fig. 5d). Calcic-amphibole occurs as xenocrysts in the lavas and can be classified as kaersutite with a compositional range of Mg# 61–72 ($n = 32$; Fig. 5c).

The earlier volcanics from the Cumbre Vieja and from the older volcanic centres in north La Palma (Taburiente, Cumbre Nueva and Bejenado) also show a wide range of clinopyroxene compositions (Lopez Ruiz 1973; Brändle et al. 1974; Klügel et al. 2000, 2005; Nikogosian et al. 2002; Galipp et al. 2006). The majority of the available analyses for the Cumbre Vieja rift zone are from pyroxene rims that have intermediate to high Al_2O_3 and TiO_2 contents and low FeO and Na_2O contents when compared with the range of clinopyroxene from the 1971 Teneguía eruption, which suggests the older Cumbre Vieja clinopyroxene populations also contain aluminium augite (Fig. 7e, f). The clinopyroxene phenocrysts from the northern volcanic centres (Taburiente, Cumbre Nueva and Bejenado) are also mostly rim analyses, which show a wide range in Al_2O_3 and TiO_2 similar to the 1971 lavas and are also restricted to low FeO and Na_2O, which suggests that aluminium augite was prevalent but sodic-augite was rare (Fig. 7e, f).

The leucogabbro xenolith is dominantly composed of plagioclase with An content of 60–79 % ($n = 79$; Fig. 5). Green pyroxene spans the augite-diopside boundary with $Wo_{42–47}En_{30–44}Fs_{12–26}$, Mg# 54–79 and high contents of FeO and Na_2O that trend towards sodic-augite-diopside ($n = 94$; Figs. 5b, 6). Calcic-amphiboles have been classified according to Leake et al. (1997). Calcic-amphibole crystals are dominantly kaersutite, with minor pargasite and edenite Mg# 51–66 ($n = 49$; Fig. 5c). Moreover, hauyne ($Ca_{1.5–1.8}Na_{3.7–4.1}K_{0.2–0.3}Al_{5.4–5.8}Si_{5.8–6.0}O_{24}$), titanite ($Ca_{0.98–0.99}Ti_{0.90–0.92}Si_{1.00–1.01}O_4$), apatite ($Ca_{3.7–3.9}PO_4$) and magnetite (40–49 % Usp) occur, along with accessory analcime, nepheline, melilitite and olivine.

The kaersutite cumulate xenoliths exhibit olivine with Fo content of 75–84 % and a mean Fo content of 78 ± 3 % and CaO of 0.13 ± 0.14 wt% (2s.d.; $n = 241$; Fig. 5a). Clinopyroxene ranges from colourless to green and is classified as diopside to augite ($Wo_{43–49}En_{38–46}Fs_{7–16}$), with Mg# of 70–87 and a mean Mg# of 77.1 ± 5.5 (2s.d.; $n = 406$; Figs. 5b, 6). The FeO content ranges from 4.4 to 8.8 wt% and Al_2O_3 from 0.5 to 9.7 wt%, ranging from

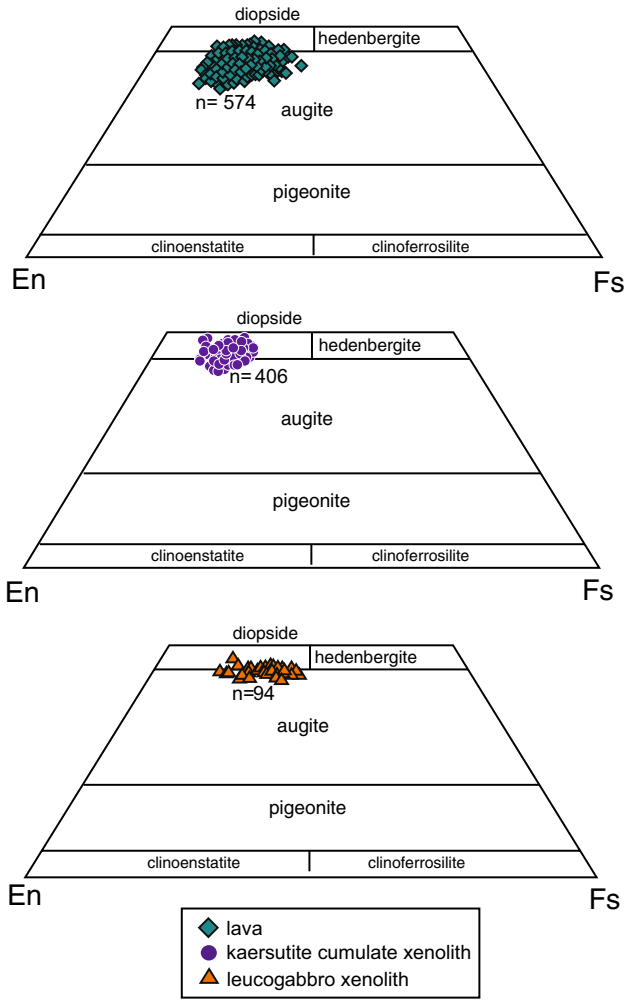

Fig. 6 Classification of clinopyroxene in the lavas, kaersutite cumulate xenoliths and leucogabbro xenolith from the 1971 Teneguía eruption (classification after Lindsley 1983)

diopside-augite to sodic and aluminium diopside, and likely explains the observed variations in colour. Calcic-amphiboles in the kaersutite cumulate xenoliths are dominantly kaersutite ($n = 342$) with minor magnesio-hastingsite ($n = 9$). The compositions range in Mg# from 49 to 75 for the kaersutite and magnesio-hastingsite (Fig. 5c). Additionally, minor phlogopite ($K_{1.46–1.52}Na_{0.23–0.29}(Mg_{3.49–3.84}Fe_{1.00–1.22}Ti_{0.42–0.54})Al_{2.14–2.24}Si_{5.04–5.10}O_{20}$), magnetite (36–48 % Usp), ilmenite (86.1–87.7 % Ilm) and accessory apatite are observed.

Whole-rock geochemistry

The Teneguía lavas are classified as basanites according to the total-alkali and silica classification scheme (Fig. 8a). They have MgO contents of 8.0–8.6 wt%, which decrease with CaO (from 11.7 to 11.0 wt%) and increase with SiO_2 (from 42.5 to 43.4 wt%) (Fig. 8). The lavas have similar compositions to the products of the second phase of the 1971 Teneguía eruption described by Ibarrola (1974) (Fig. 8). Slight decreases in Ni and Cr with MgO content are also observed. In contrast, the kaersutite cumulate xenoliths are all highly magnesian (MgO 10.7–17.0 wt%; Fig. 8), with scattered major element compositions. Although relatively scattered, some of the kaersutite cumulate xenoliths plot close to the high-Mg volcanics that extend to 13 wt% MgO, and a corresponding pre-historic suite of high-Mg basanites is found in the south of La Palma (cf. Praegel and Holm 2006).

The Teneguía lavas, like other volcanics from the Cumbre Vieja rift zone, are LREE enriched with varied LILE and notably depleted Ba and K (Fig. 8f). The kaersutite cumulate xenoliths have slightly less enriched trace element profiles than the Teneguía lavas. They show depleted Rb, Th and K relative to the Cumbre Vieja volcanics (Fig. 8f). Notably, the pre-historic high-Mg basanites from the south of La Palma show a similar to more enriched geochemical pattern compared to the kaersutite cumulate xenoliths (Praegel and Holm 2006).

Discussion

The magma plumbing system

The lavas of the 1971 Teneguía eruption provide a record of magma storage beneath the Cumbre Vieja rift zone. Additionally, the suite of xenoliths in the lavas provides the opportunity to collect further information on the magma storage system and assess their relationship with the host lavas. Thus, we applied single-mineral and mineral-melt equilibrium thermobarometry to the lavas and xenoliths. The Teneguía lavas and their xenoliths are alkaline; therefore, we used the model of Putirka et al. (2003) for clinopyroxene-melt equilibrium thermobarometry. This model is most suited to the volcanic products from La Palma, as it is calibrated to include alkaline systems that are widespread in the Canary Islands. In addition, we applied the new Masotta et al. (2013) clinopyroxene-melt model to the leucogabbro xenolith, because it is specifically calibrated for trachyte-phonolite compositions. These clinopyroxene-melt thermobarometry formulations are based on jadeite-diopside-hedenbergite exchange for temperature estimates and jadeite equilibrium crystallisation for pressure estimates (Putirka et al. 2003; Masotta et al. 2013). We also employed the plagioclase-melt equilibrium thermobarometer of Putirka (2008) for plagioclase in the lavas and leucogabbro xenolith. This method is based on temperature- and pressure-sensitive compositional and volumetric changes associated with anorthite-albite exchange. In addition, calcic-amphiboles have been used for single-crystal

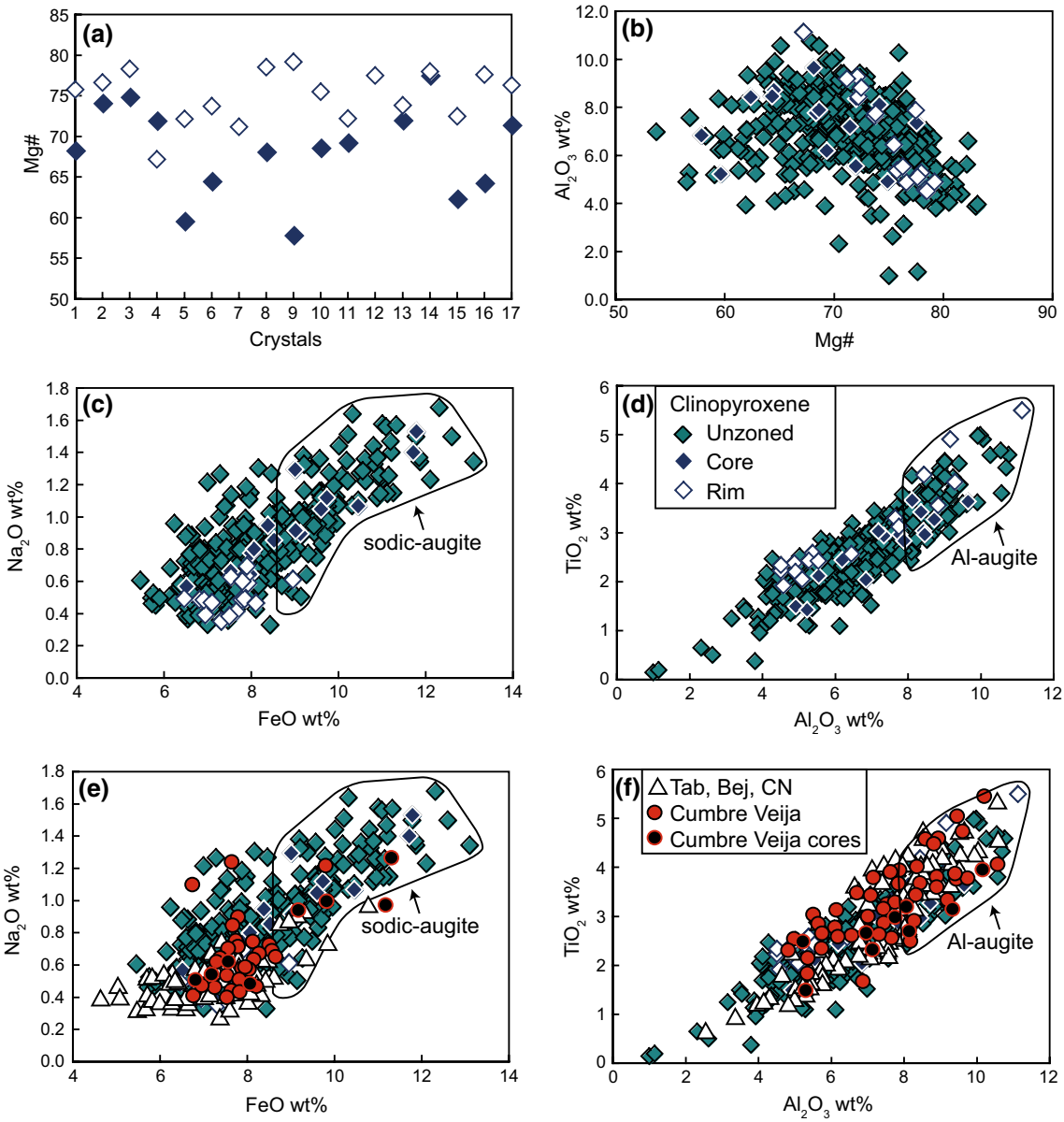

Fig. 7 Clinopyroxene mineral chemistry of the 1971 Teneguía lavas. The majority of the population were homogeneous clinopyroxene phenocrysts. Internal zoning was detected in 17 of the 557 analysed crystals. **a** Mg# for cores and rims. **b** Al_2O_3 versus Mg#, **c** Na_2O versus FeO content showing the presence of sodic-augite compositions and **d** TiO_2 versus Al_2O_3 content. Sodic-augite and aluminium augite are classified by concentrations of FeO > 8.5 wt% and Al_2O_3 > 8 wt%, respectively (see text for details). Na_2O versus FeO and TiO_2 versus Al_2O_3 show positive trends, whereas Al_2O_3 increases to a maximum of 11.5 wt% at a Mg# of 68 and then decreases as Mg# continues to decrease. These data suggest that the aluminium augite has intermediate Mg#, whereas lower-Mg# compositions are mainly sodic-augite

thermobarometry, appropriate for alkaline systems, by employing the thermobarometry formulation of Ridolfi and Renzulli (2012), which requires the input of Si, Ti, Al, Fe, Mg, Ca, Na and K composition to the pressure–temperature equations.

These geobarometric models and empirical formulations are associated with uncertainties for clinopyroxene-melt barometry of ±0.17 GPa for Putirka et al. (2003), ±0.115 GPa for Masotta et al. (2013) and ±0.3 GPa for plagioclase-melt barometry (Putirka 2008). Uncertainties associated with amphibole barometry are established from regression analysis to be ±11.5 % (Ridolfi and Renzulli 2012).

The best equilibrium fit for clinopyroxene and melt is determined by Fe–Mg partitioning and subsequent comparison of measured versus predicted diopside-hedenbergite, Ca-Tschermak, jadeite and enstatite-ferrosilite components

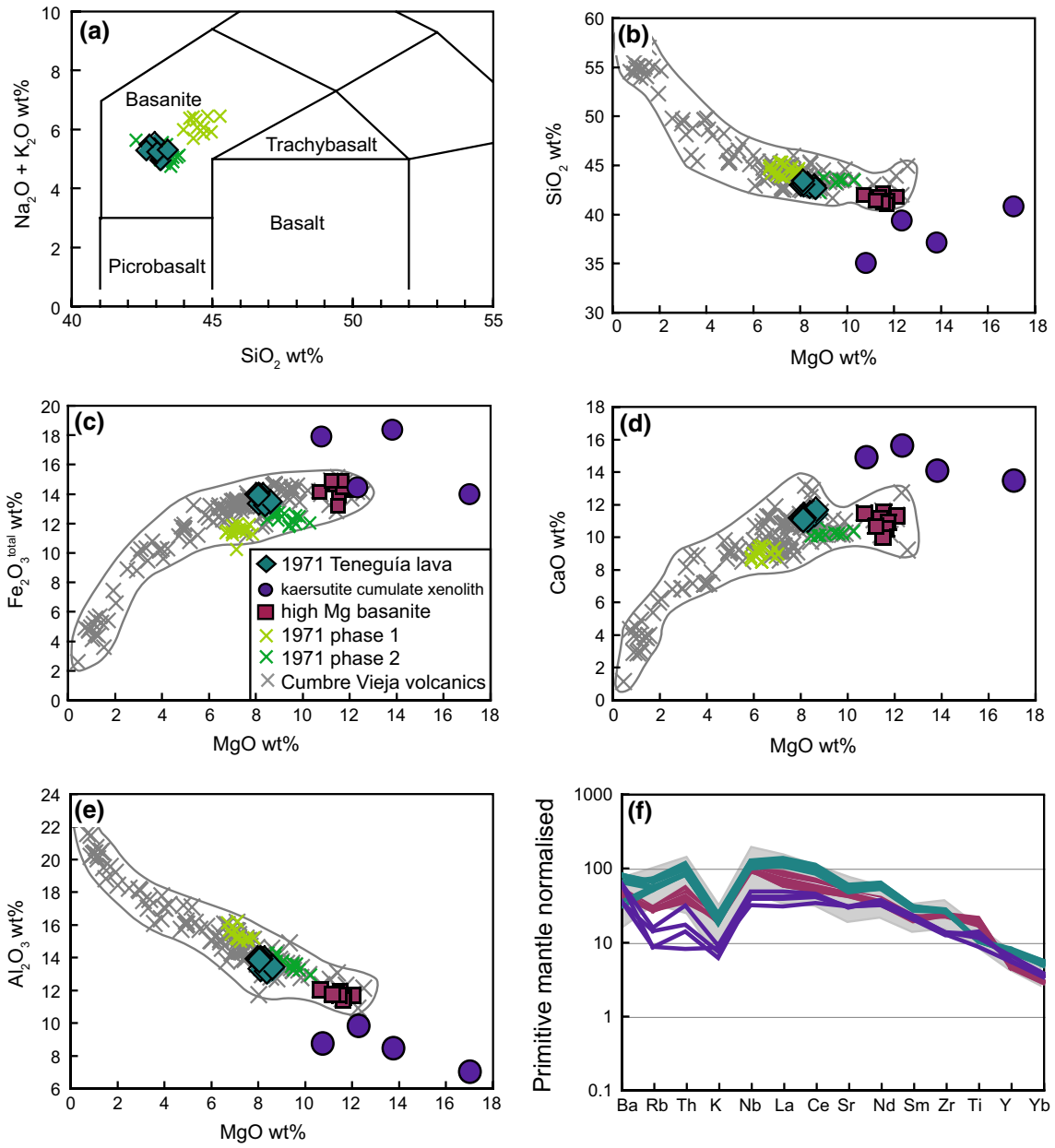

Fig. 8 Major and trace element geochemistry for the lavas and kaersutite cumulate xenoliths from the 1971 Teneguía eruption. **a** Total-alkali versus silica diagram (after Le Bas and Streckeisen 1991), **b** SiO_2, **c** Fe_2O_3, **d** CaO and **e** Al_2O_3 versus MgO, **f** primitive mantle-normalised multi-element plot (Sun and McDonough 1989). High-Mg basanites that erupted close to the 1971 Teneguía lavas and the earlier Cumbre Vieja volcanics are plotted for comparison (Praegel and Holm 2006; Carracedo et al. 2001; Klügel et al. 2000). Whole-rock geochemistry data for the leucogabbro xenolith are absent due to insufficient sample size

(Fig. 9 and supplementary figure). For plagioclase, partitioning of An and Ab between plagioclase and melt is used to assess equilibrium (Fig. 9h). Weis et al. (2015) observe parental water contents of 0.58–1.13 wt% for magmas from La Palma, based on reconstruction of water contents from dehydrated clinopyroxene. Therefore, we have considered a range of water contents from 0 to 1 % H_2O for plagioclase thermobarometry, consistent with water contents for Ocean Island Basalts globally (e.g. Wallace 2005; Kovalenko et al. 2007). Variation of water within this range made little difference; hence, only thermobarometric models for water contents of 0.5 % are presented.

Oxygen fugacity has been calculated from magnetite–ilmenite pairs coexisting in the kaersutite cumulate xenoliths to be +0.49 to −2.24 log units around FMQ (Lindsley and Spencer 1982; Frost 1991; Lepage 2003). The calculated values are comparable to oxygen fugacity of basanites from the 1949 eruption presented by Klügel et al. (2000). In

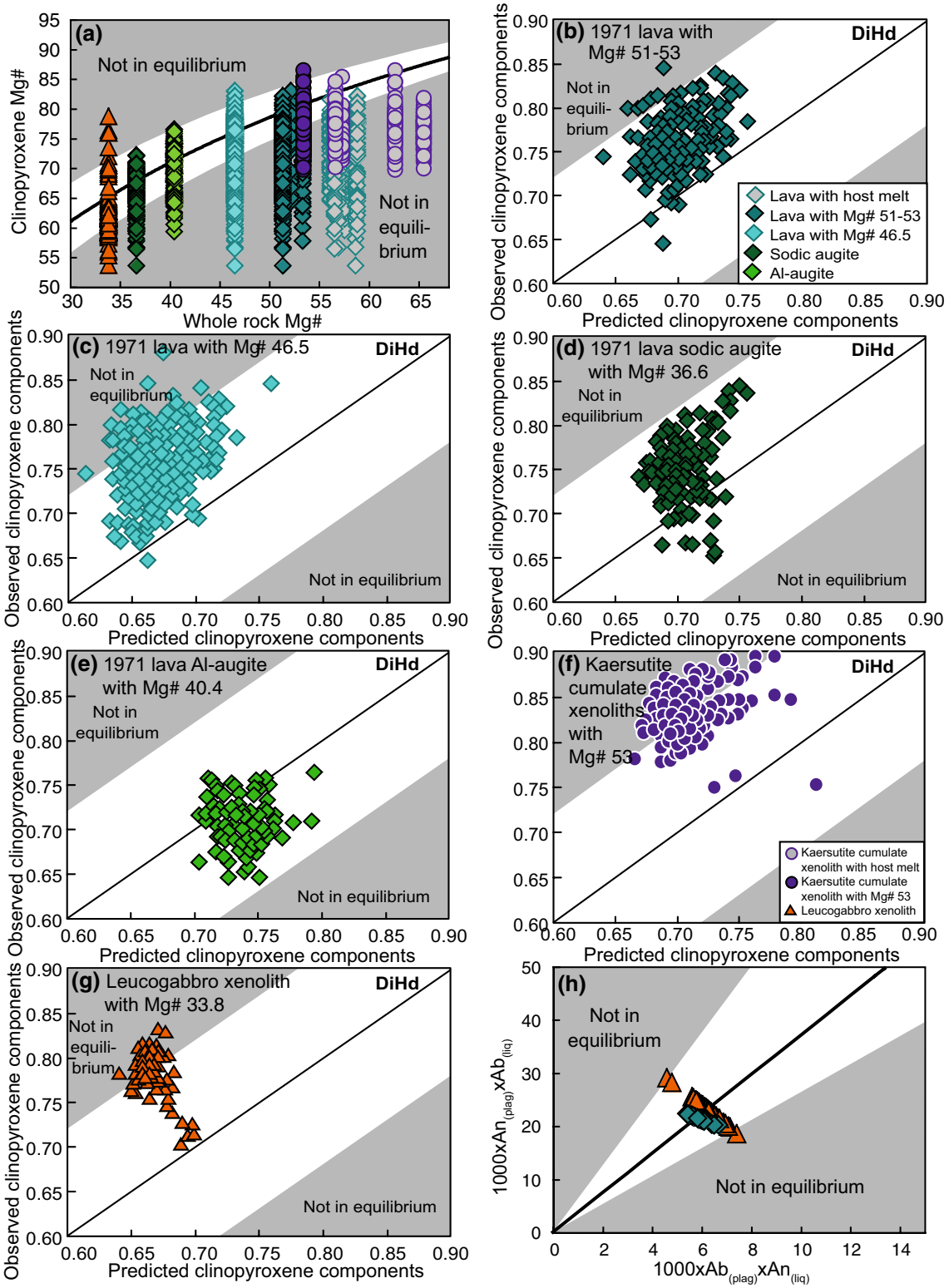

Fig. 9 Clinopyroxene-melt and plagioclase-melt equilibrium tests; **a** Fe–Mg partitioning in clinopyroxene. Equilibrium associated with diopside-hedenbergite (DiHd), components of pyroxene is shown for **b** diopside in the lavas paired with melts of Mg# 51–53, **c** diopside in the lavas paired with melts of Mg# 46.5, **d** sodic-augite in the lavas, **e** aluminium augite in the lavas, **f** clinopyroxene in the kaersutite cumulate xenoliths, and **g** clinopyroxene in the leucogabbro xenolith. **h** Plagioclase-melt equilibrium is illustrated by An–Ab partitioning in plagioclase. The equilibrium envelope for Fe–Mg partitioning is $Kd^{(Fe-Mg)} = 0.275 \pm 0.067$ Putirka et al. (2003) and for Di–Hd exchange ±0.12 2SEE (Putirka 1999). See supplementary figure for EnFs, CaTs and Jd component equilibrium. Nominal melt compositions for clinopyroxene and plagioclase are selected from whole-rock compositions from this study and from Carracedo et al. (2001), Praegel and Holm (2006) and Weis et al. (2015)

addition, Ocean Islands have been observed to show Fe^{3+}/Fe_{total} between 0.15 and 0.25 (Herzberg and Asimow 2008). An Fe^{3+}/Fe_{total} of 0.21 has therefore been used to recalculate whole-rock compositions (cf. Barker et al. 2009).

Unfortunately, the matrix was too crystalline to provide suitable analyses of the melt composition, and moreover, the different populations of clinopyroxene that are juxtaposed require a range of melt compositions (Fig. 3). Therefore, the matrix would not be expected to record the melt that an adjacent clinopyroxene actually grew from. Melt inclusions were also avoided due to the likelihood of providing compromised melt compositions due to post-emplacement modification (Baker 2008).

Nominal melts have been selected from the whole-rock compositions of the associated lavas and from the additional literature data (Carracedo et al. 2001; Praegel and Holm 2006; Weis et al. 2015), following procedures similar to Putirka (1997), Mordick and Glazner (2006) and Dahren et al. (2012). Likewise, whole-rock analyses of kaersutite cumulate xenoliths, supplemented by data for lavas from Weis et al. (2015), have been used as equilibrium melts for the kaersutite cumulate xenoliths. In a similar manner, equilibrium melt compositions for the leucogabbro xenolith have been selected from representative phonolite melt compositions from Carracedo et al. (2001) and Praegel and Holm (2006). Where the whole-rock composition is not an appropriate nominal melt, an iterative process has been used to choose a suitable equilibrium melt composition from whole-rock data presented in the literature. This involved checking for melts with suitable Mg# for equilibrium Mg–Fe partitioning (Fig. 9a), and then for fit with Ca–Na–Al composition by using the predicted versus observed clinopyroxene components equilibrium method (Fig. 9 and supplementary figure). Whole-rock compositions that did not result in clinopyroxene component equilibrium were discarded, and another melt with similar Mg# was tested. This cycle was repeated until an appropriate composition that satisfies both equilibrium conditions was found. Other evidence that supports the equilibrium is a comparison between clinopyroxene and amphibole thermobarometry in the xenoliths, which are consistent. Moreover, comparison between pressure estimates from Klügel et al. (2000) and our recalculation of their data using a whole-rock composition as an equilibrium melt produces very similar pressures when applying the Putirka et al. (1996) thermobarometer (see below).

Pressures have been converted to depths using a two-tiered density model with 2800 kgm^{-3} for the approximately 14 km mafic oceanic crust (Ranero et al. 1995) and a deeper layer with an average upper mantle density of 3111 kgm^{-3}, which is considered to be representative of the surrounding oceanic lithospheric mantle (Tenzer et al. 2013).

The Teneguía lavas

The equilibrium tests for the Teneguía lavas and their associated minerals show that only a small proportion of the clinopyroxene phenocrysts are in Fe–Mg equilibrium with their respective host rock compositions (n = 15/574; Fig. 9a). However, the number of equilibrium pairs increases when clinopyroxene is coupled with whole-rock compositions of between Mg# 51 and 53 (n = 225; samples LP1971-1 and LP1971-3; Weis et al. 2015). A larger proportion of clinopyroxene satisfies equilibrium conditions with a whole-rock composition of Mg# 46.5 (n = 346; sample 116,504; Praegel and Holm 2006) (Fig. 9a). The clinopyroxene compositions in equilibrium with whole-rock compositions of Mg# 51–53 are Mg# ≥75, and for equilibrium with a whole-rock composition of Mg# 46.5, the clinopyroxene phenocrysts have Mg# ≥72. The clinopyroxene phenocrysts in Fe–Mg equilibrium are also observed to meet equilibrium conditions for measured versus predicted diopside-hedenbergite, Ca-Tschermak, jadeite and enstatite-ferrosilite components (Fig. 9b, c and supplementary figure). Considering the other populations of clinopyroxene in these samples, we demonstrate that sodic-augite compositions with FeO_{total} > 8.5 wt% and Mg# 65–77 are observed to be in Fe–Mg and clinopyroxene component equilibrium with a whole-rock composition of Mg# 36.6 (n = 150; sample 71; Carracedo et al. 2001) (Figs. 7, 9a, d). In turn, aluminium augite compositions with Al_2O_3 > 8 wt% and Mg# 68–76 are in Fe–Mg equilibrium as well as measured versus predicted clinopyroxene component equilibrium with a whole-rock composition of 40.4 Mg# (n = 99; sample 279; Carracedo et al. 2001) (Figs. 7, 9a, e). In addition, plagioclase with An 60–70 % appears to be in equilibrium with a whole-rock composition of Mg# 51.3 (Fig. 9h; n = 23) (sample LA1971-1; Weis et al. 2015).

The equilibrium mineral-melt data were modelled by employing the thermobarometric formulations of Putirka et al. (2003). The clinopyroxene in equilibrium with melt compositions of Mg# 51–53 crystallised at temperatures of 1147–1210 °C with a mean of 1175 ± 20 °C (2s.d.) and pressures of 0.64–1.41 GPa, with a mean of 0.98 ± 0.26 GPa (2s.d.: Fig. 10a), equating to depths of 30–45 km (Fig. 11a). Clinopyroxene in equilibrium with a melt composition of Mg# 46.5 in turn crystallised at temperatures of 1078–1202 °C with a mean of 1111 ± 41 °C (2s.d.) and pressures of 0.53–1.36 GPa with a mean of 0.89 ± 0.28 (2s.d.; Fig. 10a), equivalent to depths of 25–40 km (Fig. 11a). The rare plagioclase phenocrysts appear to have crystallised at temperatures of 1114 ± 5 °C (2s.d.) and pressures of 1.07 ± 0.06 (2s.d), translating to depths of approximately 40 km (Fig. 11a). Relatively high depths of plagioclase crystallisation suggest stabilisation by high water

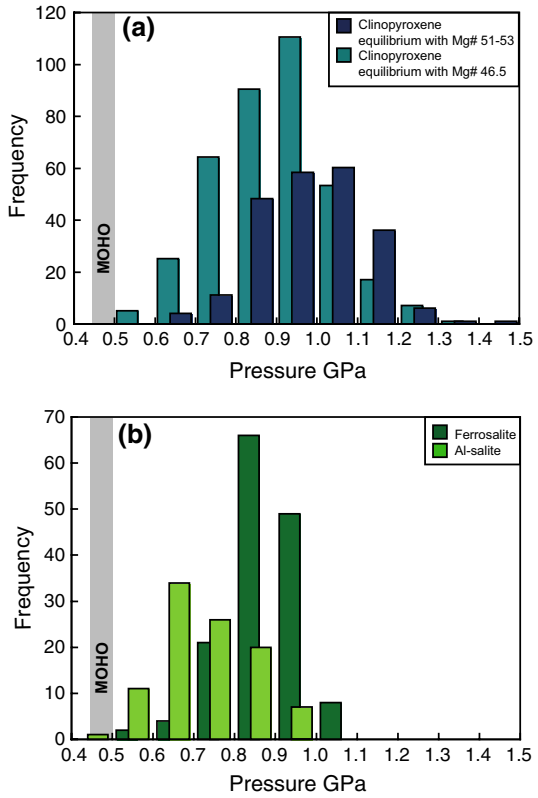

Fig. 10 Crystallisation pressures for clinopyroxene from the 1971 Teneguía lavas. **a** Diopside paired with equilibrium melts of Mg# 51–53 and 46.5, **b** sodic-augite and aluminium augite paired with equilibrium melts of Mg# 36.6 and 40.4, respectively. The Moho is shown as a *vertical grey bar* for comparison (Ranero et al. 1995)

pressures, which is consistent with the growth of calcic-amphibole in the alkaline lithospheric mantle. Xenocrysts of calcic-amphibole in the lavas record crystallisation pressures of 0.92 ± 0.39 GPa (2s.d.; Ridolfi and Renzulli 2012) and, thus, a depth range similar to that for clinopyroxene crystallisation (25–40 km; Fig. 11a). Sodic-augite crystallised at 1001–1032 °C with a mean of 1020 ± 12 °C (2s.d.) and 0.55–1.06 GPa with a mean of 0.87 ± 0.18 (2s.d., Fig. 10b), also overlapping with clinopyroxene crystallisation at depths of 27–37 km (Fig. 11a). Aluminium augite, which typically records processes of ascent (Kushiro 1962), crystallised at temperatures of 1062–1096 °C with a mean of 1082 ± 14 °C (2s.d.) and pressures of 0.47–0.99 GPa, with a mean of 0.73 ± 0.22 (2s.d., Fig. 10b), equating to depths of 20–35 km (Fig. 11a), thus indeed reflecting slightly shallower depths than the other clinopyroxenes.

In addition to the observation that all populations of clinopyroxene are present in all investigated samples, each clinopyroxene population in an individual sample spans a similar range to the total range in clinopyroxene compositions (Fig. 7). Furthermore, the sample averages are consistent with the highest frequencies for the total range in clinopyroxene compositions (Fig. 10). The variance of clinopyroxene crystallisation pressure for each population within individual samples ranges from 0.12 to 0.36 GPa 2s.d., which is mostly greater than the standard error of estimate 0.17 GPa. Thus, the majority of the samples and clinopyroxene populations display a range of crystallisation pressures that exceed the uncertainties of the method and suggest that the pressure variations are robust. Since the clinopyroxene compositions in our data set span a larger compositional range than Galipp et al. (2006) and Klügel et al. (2000, 2005), our estimated pressures naturally display a wider range and hence provide information, not only on the upper parts of the storage system, but also on the entire magma plumbing system.

The local Moho resides at 0.4–0.5 GPa (ca. 14 km; Ranero et al. 1995), indicating that the dominant crystallisation recorded by the 1971 Teneguía lavas was relatively deep in the oceanic lithospheric mantle. Crystallisation of sodic-augite at similar depths to the main clinopyroxene crystallisation level suggests that magmas with ca. 6.5 wt% MgO differentiated to magmas with 3.1 wt% MgO at this level in the lithospheric mantle. Although the overlap in uncertainties is considerable, the aluminium augite shows a range of pressures that extends to slightly shallower depths than the main clinopyroxene crystallisation zone, implying the presence of additional sub-Moho magma pockets that have a more evolved character (Figs. 10b, 11a). The diverse crystal populations and the relatively wide range of compositions in individual samples suggest that clinopyroxene and plagioclase were formed in multiple small magma batches over a range of depths in the oceanic lithosphere. The small magma pockets were likely amalgamated shortly before ascent from the oceanic lithospheric mantle magma storage system. Different magma pockets would have had different residence times providing a range of phenocryst sizes, with the smaller minerals, such as plagioclase, likely representing shorter residence times.

Xenoliths in the Teneguía lavas

The kaersutite cumulate xenoliths host clinopyroxene with a wide range of compositions; however, when we test for equilibrium with the host rock, we find that few are in equilibrium with such a high-Mg# melt (Fig. 9a). When matched with a melt composition of Mg# 53, equilibrium vastly improves such that 218 single analyses of clinopyroxene with Mg# 77.5–85 are in equilibrium with this selected melt (Fig. 9a, f and supplementary figure; sample LA1971-3; Weis et al. 2015). In addition, the clinopyroxene in the leucogabbro xenolith shows best equilibrium fit with a whole-rock composition of Mg# 33.8, where the highest clinopyroxene data density falls in the equilibrium envelope between Mg# of 60 and 71 (Fig. 9a, g; Carracedo

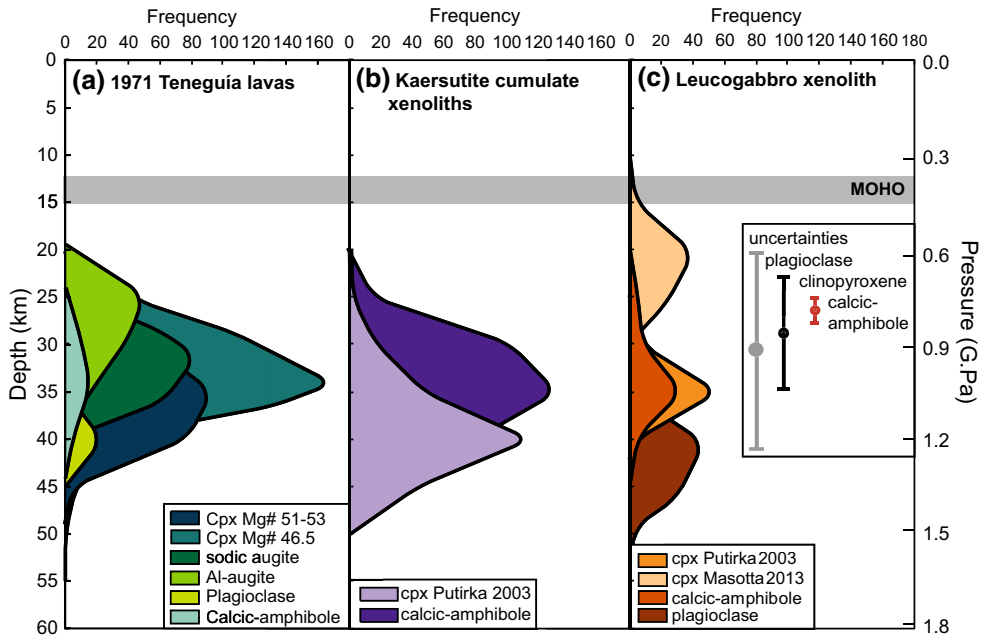

Fig. 11 Schematic crystallisation depth distribution for the 1971 Teneguía lavas and xenoliths. **a** The 1971 Teneguía lavas, **b** kaersutite cumulate xenoliths, **c** leucogabbro xenolith. Clinopyroxene-melt and plagioclase-melt thermobarometers according to Putirka et al. (2003), Masotta et al. (2013) and Putirka (2008) have been employed. Calcic-amphibole pressures have been calculated with the amphibole thermometer of Ridolfi and Renzulli (2012), which is suitable for alkaline magmatic systems. Depths have been calculated using a two-tiered density model with 2800 kgm^{-3} below the Moho and a density of 3111 kgm^{-3} for the lithospheric mantle (Tenzer et al. 2013). The Moho is located at 14 km (Ranero et al. 1995)

et al. 2001). In turn, plagioclase in the leucogabbro shows equilibrium with a melt with Mg# 46.5 (Fig. 9h; sample 116,504; Praegel and Holm 2006).

Application of the barometric models from Putirka et al. (2003) and Ridolfi and Renzulli (2012) indicates that the kaersutite cumulate xenoliths host clinopyroxene that crystallised at mean temperatures of 1174 ± 22 °C (2s.d.), mean pressures of 1.09 ± 0.28 GPa (2s.d.), and the majority of the pressures translate to depths of 35–45 km (n = 218; Fig. 11b). The calcic-amphiboles have crystallisation temperatures of 1179 ± 150 °C and pressures averaging 0.96 ± 0.30 GPa (2s.d.) and equate to depths of 25–40 km (n = 346; Fig. 11b). Thus, the magma that gave rise to the kaersutite cumulate xenoliths appears to have crystallised relatively deep in the lithosphere, commencing with clinopyroxene that was followed by slightly shallower calcic-amphibole growth.

The plagioclase in the leucogabbro crystallised at 1104 ± 9 °C and 1.20 ± 0.14 GPa (2s.d.; n = 79), whereas clinopyroxene in the leucogabbro crystallised at 1026 ± 8 °C, 0.67–1.07 GPa and 0.35–0.68 GPa using the Putirka et al. (2003) and Masotta et al. (2013) geobarometers, respectively (2s.d.; n = 65; Fig. 11c). Corresponding calcic-amphibole crystallisation occurred at temperatures of 1094 ± 134 °C and pressures of 0.89 ± 0.32 GPa (n = 49), which equates to crystallisation depths of plagioclase, clinopyroxene and calcic-amphibole between approximately 30 and 50 km for the leucogabbro. Plagioclase with high An contents of 60–79 % are coupled with a melt composition of Mg# 46.5 and crystallised deep (35–45 km), whereas more evolved sodic-augite-diopside and calcic-amphibole with Mg# 51–79 and equilibrium with a more evolved melt of Mg# 33.8 are associated with shallower crystallisation (30–40 km), thus providing evidence for progressive magmatic differentiation on ascent through the oceanic lithospheric mantle.

Integrating the information derived from the xenoliths with the lavas, we find that the 1971 Teneguía lavas record plagioclase and clinopyroxene crystallisation at depths of 20–45 km and therefore relatively deep in the lithosphere (Fig. 11). The magmas feeding the 1971 Teneguía eruption have intercepted kaersutite cumulates and plutonic leucogabbro during magma storage deep in the oceanic lithospheric mantle, where the magma collected kaersutite cumulate and leucogabbro xenoliths. The magmas have then ascended towards the Moho crystallising aluminium augite (20–35 km).

It is uncertain when the magmas mixed to distribute all clinopyroxene populations across all samples. Given the trends between populations from low to high Al_2O_3 and TiO_2 (Fig. 7), opposed to discreet populations, it is likely that each small magma batch pooled frequently during

ascent through the lithosphere, evolving and growing clinopyroxene phenocrysts that are successively enriched in Al_2O_3, TiO_2 and lower in MgO. The trends in Na_2O and FeO also suggest that separate small magma batches continuously evolved during ascent and thus were likely juxtaposed as the aluminium augite grew prior to ascent. In this scenario, the xenoliths would have been collected and pooled together with the host magma during formation of aluminium augite, which led to disaggregation of the xenoliths to form glomerocrysts and xenocrysts and partial digestion of the leucogabbro xenoliths such that they became rarer and smaller than the kaersutite cumulate xenoliths.

The connection between kaersutite cumulate xenoliths and high-Mg lavas

The kaersutite cumulate xenoliths hosted by the 1971 Teneguía lavas provide a record of the older parts of the Cumbre Vieja magmatic system, which can be used to assess the relationship with earlier erupted Cumbre Vieja products.

The 1971 Teneguía lavas are basanites with 8–8.6 wt% MgO and are enriched in HFSE and LREE, but depleted in Ba and K, similar to most of the earlier Cumbre Vieja volcanics (Fig. 8). In contrast, the kaersutite cumulate xenoliths show high MgO contents and low LILE. The presence of kaersutite in the kaersutite cumulate xenoliths suggests that the low LILE concentrations are a result of removal of K-, Rb-, Ba-bearing phases, such as calcic-amphibole, by fractional crystallisation and subsequent formation of the cumulates by crystal accumulation. Accumulation of clinopyroxene, olivine and kaersutite is required to produce the elevated MgO, CaO and scatter in the major elements as well as Rb and Th that characterise the kaersutite cumulate xenoliths (Fig. 8).

The majority of the volcanics from Cumbre Vieja have not undergone amphibole fractionation and are thus not likely to represent parental magmas of the kaersutite cumulates and cannot be considered cognate with the 1971 lavas per se. Instead, a parental magma to the kaersutite cumulates would be expected to have high MgO content and depleted LILE composition. The rare high-Mg lavas from La Palma are a suitable analogue for the parental magma to the kaersutite cumulates, and a geographically proximal suite of pre-historic high-Mg lavas is observed in the South Cumbre Vieja rift zone near to the 1971 Teneguía lavas (Fig. 8; Carracedo et al. 2001; Praegel and Holm 2006). Notably, the major element and LILE compositions of these high-Mg lavas are intermediate between those of the 1971 Teneguía lavas and the kaersutite cumulate xenoliths, which likely reflect the formation of the high-Mg kaersutite cumulate xenoliths from a high-Mg magma at depth (Fig. 8). Part of this high-Mg magma was probably erupted forming the pre-historic high-Mg lavas of south La Palma, while the residue accumulated at depth to form cumulate suites. Later, the magmas feeding the 1971 Teneguía eruption picked up high-Mg kaersutite cumulate xenoliths from these cumulate suites. The eruption of the older high-Mg lavas at the southwest corner of La Palma (Fig. 2), in the geographical proximity of the 1971 vent complex, thus implies a reused magma plumbing system for the pre-historic and recent Cumbre Vieja eruptions in the south of the island, consistent with studies on the earlier Cumbre Vieja rift zone (Klügel et al. 2005).

Magma–lithosphere interaction

The lavas of the 1971 Teneguía eruption have undergone magma–lithosphere interaction on a number of scales. Firstly, and most obviously, the 1971 Teneguía lavas have entrained xenoliths of kaersutite cumulate and leucogabbro lithologies. Secondly, magma–lithosphere interaction is observed through the incorporation of calcic-amphibole xenocrysts and glomerocrysts in the 1971 Teneguía lavas (Fig. 3d). Calcic-amphibole has been observed in all of the 1971 lava samples and always shows resorption, rounded edges and selvages, implying that the amphibole crystals are in disequilibrium and are probably derived from either the kaersutite cumulates or leucogabbro assemblages. Notably, the compositions (Mg#) of the calcic-amphibole in xenocrysts and glomerocrysts overlap with those in the kaersutite cumulates (Fig. 5c). Additionally, crystallisation pressures of the calcic-amphibole xenocrysts coincide with the peak crystallisation pressures for the kaersutite in the kaersutite cumulates (Fig. 11). Although the calcic-amphibole xenocrysts appear to be derived from kaersutite cumulate assemblages, observed xenocrysts of low An plagioclase, titanite, apatite and aegirine-augite are likely derived from a more evolved, leucogabbro assemblage. Hence, the 1971 Teneguía lavas record assimilation of kaersutite cumulates and leucogabbro from the deeper levels of the plumbing system, implying that the magmatic conduits follow similar paths to those of earlier Cumbre Vieja magmas in this area. Thus, recycling of the young Ocean Island plutonic complex deep beneath the Cumbre Vieja rift zone is suggested.

Temporal evolution of the La Palma magmatic plumbing system

In order to shed more light on the temporal development of La Palma's magmatic plumbing system, we now put the observations from the 1971 Teneguía eruption in context with the geological history of La Palma. We compare the magma storage conditions of the 1971 Teneguía lavas with the earlier volcanic products of the Cumbre Vieja rift zone

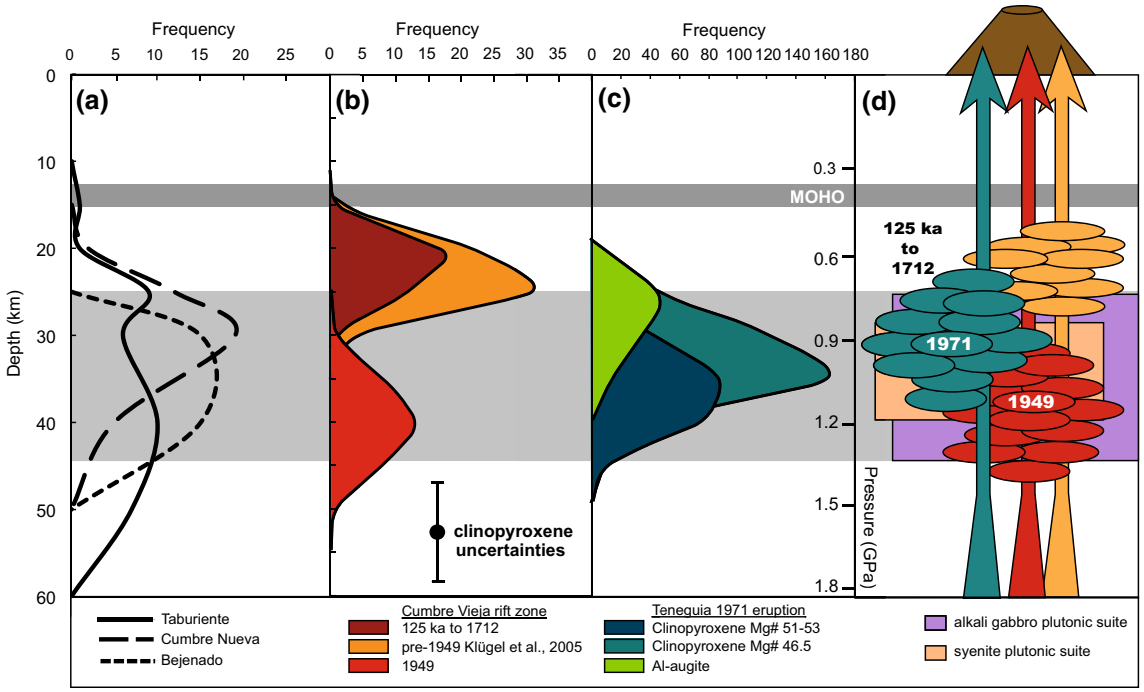

Fig. 12 Schematic representation of the development of the magmatic plumbing system beneath La Palma. **a** Compilation of averaged clinopyroxene thermobarometry data from the pre-historic Taburiente, Cumbre Nueva and Bejenado volcanoes that cluster at crystallisation depths of 25–45 km (Galipp et al. 2006). **b** Averaged clinopyroxene thermobarometry of pre-historic and historic eruptions at the Cumbre Vieja rift zone shows crystallisation depths of 15–30 km, whereas the recent 1949 lava records clinopyroxene crystallisation at ca. 35–45 km (Klügel et al. 2000, 2005). **c** The 1971 Teneguía lavas record clinopyroxene crystallisation depths of 25–45 km, similar to the magmas that fed the 1949 eruption. **d** Schematic evolution of the successive magmatic plumbing systems beneath La Palma. The *light grey* field marks the dominant depths of clinopyroxene crystallisation of the Taburiente, Cumbre Nueva and Bejenado volcanoes. The Moho is plotted as a *horizontal bar* at approximately 14 km (Ranero et al. 1995). A tendency towards deeper storage beneath the Cumbre Vieja is noted for the 1949 and 1971 lavas suggesting a potential role for progressive underplating beneath the Cumbre Vieja

as well as the older northern volcanic complexes of Taburiente, Cumbre Nueva and Bejenado.

In order to do so, a data set for the older volcanics from La Palma was compiled from existing mineral data (Lopez 1973; Brändle et al. 1974; Nikogosian et al. 2002; Galipp et al. 2006; Klügel et al. 2000, 2005). To ensure the data processing is consistent between the older data sets and our 1971 Teneguía data, the nominal melts were selected using the same procedure of matching the Mg# and the clinopyroxene components of the minerals with whole-rock compositions as has been performed for our 1971 samples (see above). We employed an additional test for equilibrium by the comparison of the pressure data with the results of Klügel et al. (2000). Our results for the 1949 eruption gave pressures of 0.48–1.07 GPa when using the Putirka et al. (1996) model, which is very close to the pressures of 0.44–1.11 GPa reported in Klügel et al. (2000), confirming the equilibrium between mineral and whole-rock data. For consistency, we then employed the approach of Putirka et al. (2003) to all data sets from La Palma. We note that deeper estimates of crystallisation depths are derived for the 1949 eruption when using Putirka et al. (2003) as compared to the Putirka et al. (1996) formulation, which reflects the systematic offset between the thermobarometry formulations of Putirka et al. (1996) and Putirka et al. (2003) and the improved accuracy provided by Putirka et al. (2003).

The complied clinopyroxene data sets for the Taburiente, Cumbre Nueva and Bejenado volcanoes and the Cumbre Vieja rift zone predominantly contain analyses of clinopyroxene rims and show a range in compositions from augite to aluminium augite (Fig. 7f). The pre-historic eruptions from the Taburiente, Cumbre Nueva and Bejenado volcanoes record clinopyroxene crystallisation depths of approximately 25–45 km (Fig. 12a; Galipp et al. 2006). When the magmatism later shifted to the Cumbre Vieja rift zone, clinopyroxene crystallisation appears to have been shallower at depths of 15–30 km (Fig. 12b: Klügel et al. 2005; Galipp et al. 2006), which led Galipp et al. (2006) to suggest that the magmatic plumbing system for the Cumbre Vieja rift zone was separate from the older magmatic system of the island. Subsequent Cumbre Vieja rift zone eruptions associated with the 1949 eruption carried clinopyroxene that once again appears to have formed deeper in the oceanic lithospheric mantle at ca. 35–45 km (Fig. 12b; recalculated

from Klügel et al. 2000 using Putirka et al. 2003 for internal consistency). Later, the clinopyroxene associated with the 1971 Teneguía eruption crystallised between 25 and 45 km, at comparable to slightly shallower depths to the clinopyroxene from the 1949 eruption (Fig. 12c). Therefore, it appears that the early Cumbre Vieja rift zone magmas stalled directly beneath the Moho, while the more recent magmas associated with the 1949 and 1971 events crystallised deeper and at similar levels to the magmas from the older northern volcanic centres (Fig. 12; Galipp et al. 2006). This apparent deepening of the magma plumbing system from the early Cumbre Vieja rift zone events to the recent 1949 and 1971 events is likely an indication of progressive underplating that may extend up to 10 km in that region (Klügel et al. 2005). This notion is consistent with geophysical evidence from the Canary Island archipelago (cf. Carracedo et al. 2015). At the nearby islands of Tenerife and Gran Canaria, underplating has indeed been estimated to be on the order of 10 km, which is consistent with the limited geophysical data available for La Palma (Dañobeitia and Canales 2000; Catalán et al. 2003).

The observation of magma storage in the oceanic lithospheric mantle across the Canary archipelago reflects the structure of the oceanic crust and resulting discontinuities (Longpré et al. 2008; Stroncik et al. 2009; Aulinas et al. 2010). Furthermore, comparable levels of magma storage are found in a narrow belt of the Anti-Atlas, which are thought to reflect a sublithospheric corridor associated with Canarian mantle plume flow beneath North Africa (Berger et al. 2008; Duggen et al. 2009; Miller et al. 2015).

Conclusions

The lavas from the 1971 Teneguía eruption of the Cumbre Vieja rift zone on La Palma host clinopyroxene including augite, sodic-augite and aluminium augite, olivine and minor plagioclase phenocrysts as well as xenocrystic calcic-amphibole and plagioclase. The mineral assemblage of the lavas traces the evolution of the magma plumbing system, with augite and sodic-augite crystallising relatively deep in the oceanic lithospheric mantle (25–45 km). The juxtaposition of diopside and sodic-augite, where the latter appears to have grown in equilibrium with a more evolved magma, indicates a significant differentiation in the deep magma plumbing system.

Clinopyroxene from the magmas feeding the 1971 Teneguía eruption has comparable crystallisation depths to clinopyroxene from the 1949 event, which themselves show deeper crystallisation than early Cumbre Vieja events. The progressive deepening of the magma storage system suggests that underplating of the crust is likely occurring beneath the Cumbre Vieja rift zone. The aluminium augite, in turn, records shallower crystallisation in sub-Moho magma reservoirs at depths of 20–35 km, similar to the early Cumbre Vieja magmatic systems. This and the presence of kaersutite cumulate and leucogabbro xenoliths in the 1971 Teneguía lavas provide evidence for recycling of Ocean Island plutonic sequences and implies reuse of the earlier magma plumbing systems during recent Cumbre Vieja events in the southern part of La Palma.

Acknowledgments We thank F.M. Deegan, C. Karsten, T.R. Walter and K. Zazcek for help during successive field visits. We are grateful for analytical assistance from H. Harryson and J.M. Majka at Uppsala University. Research assistants A. Svensson, T. Mattsson and C. Holloway are thanked for help with data acquisition, processing and drafting of figures. We are grateful to A. Klügel and two anonymous reviewers for valuable discussion of our work. Funding from the Swedish Research council (VR) to Barker and Troll is gratefully acknowledged. This manuscript contributes to the efforts of the Swedish Centre for Natural Disaster Sciences (CNDS).

References

Afonso A, Aparicio A, Hernández-Pacheco A, Badiola ER (1974) Morphology evolution of Teneguia volcano area. Estud Geol (Madrid) Teneguia. 19–26

Andersson UB (1997) Petrogenesis of some proterozoic granitoid suites and associated basic rocks in Sweden (geochemistry and isotope geology). SGU Rapp Medd 91:216

Araña V, Fúster VM (1974) La erupción del volcán Teneguía, La Palma, Islas Canarias. Estud Geol. (Madrid) Teneguia. 15–18

Araña V, Ibarrola E (1973) Rhyolitic pumice in the basaltic pyroclasts from the 1971 eruption of Teneguia volcano, Canary Islands. Lithos 6:273–278

Aulinas M, Gimeno D, Fernandez-Turiel JL, Perez-Torrado FJ, Rodriguez-Gonzalez A, Gasperini D (2010) The Plio-Quaternary magmatic feeding system beneath Gran Canaria (Canary Islands, Spain): constraints from thermobarometric studies. J Geol Soc 167:785–801

Baker DR (2008) The fidelity of melt inclusions as records of melt composition. Contrib Miner Petrol 156:377–395

Bakker RJ, Jansen JBH (1994) A mechanism for preferential H2O leakage from fluid inclusions in quartz, based on TEM observations. Contrib Mineral Petrol 116:7–20

Barker AK, Holm PM, Peate DW, Baker JA (2009) Geochemical stratigraphy of submarine lavas (3–5 Ma) from the Flamengos Valley, Santiago, Southern Cape Verde Islands. J Petrol 50:169–193. doi:10.1093/petrology/egn081

Berger J, Ennih N, Liégeois JP, Nkono C, Mercier JCC, Demaiffe D (2008) A complex multi-chamber magmatic system beneath a late Cenozoic volcanic field: evidence from CSDs and thermobarometry of clinopyroxene from a single nephelinite flow (Djbel Saghro, Morocco). Geol Soc Lond Special Publ 297(1):509–524

Brändle JL, Fernández Santín S, Lopez-Ruiz J (1974) Mineralogy Of the materials from Teneguía Volcano, La Palma, Canary Islands. Estudios Geol (Madrid) Teneguía. 41–47

Carracedo JC, Day SJ, Guillou H, Gravestock P (1999) Later stages of volcanic evolution of La Palma, Canary Islands: rift evolution, giant landslides, and the genesis of the Caldera de Taburiente. Geol Soc Am Bull 111(5):755–768

Carracedo JC, Badiola ER, Guillou H, De La Nuez J, Perez-Torrado FJ (2001) Geology and volcanology of La Palma and El Hierro, Western Canaries. Estud Geol (Madrid) 57:175–273

Carracedo JC, Guillou H, Nomade S, Rodríguez-Badiola E, Pérez-Torrado FJ, Rodríguez-González A, Paris R, Troll VR, Weismaier S, Delcamp A, Fernández-Turiel JL (2011) Evolution of ocean-island rifts: the northeast rift zone of Tenerife, Canary Islands. Geol Soc Am Bull 123(3–4):562–568

Carracedo JC, Perez-Torrado FJ, Rodríguez-González A, Soler V, Fernández-Turiel JL, Troll VR, Wiesmaier S (2012) The 2011 submarine volcanic eruption in El Hierro (Canary Islands). Geol Today 28(2):53–58. doi:10.1111/j.1365-2451.2012.00827.x

Carracedo JC, Troll VR, Zaczek K, Rodríguez-González A, Soler V, Deegan FM (2015) The 2011–2012 submarine eruption of El Hierro, Canary Islands: new lessons in oceanic island growth and volcanic crisis management. Earth-Sci Rev 150:168–200

Catalán M, Martin Davila J, ZEE Working Group (2003) A magnetic anomaly study offshore the Canary Archipelago. Mar Geophys Res 24:129–148. doi:10.1007/s11001-004-5442-y

Chaigneau M (1974) Gaz fumaroliens et gaz dans es lavas. Estud Geol (Madrid) Teneguia. 75–85

Dahren B, Troll VR, Andersson UB, Chadwick JP, Gardner MF, Jaxybulatov K, Koulakov I (2012) Magma plumbing beneath Anak Krakatau volcano, Indonesia: evidence for multiple magma storage regions. Contrib Miner Petrol 163:631–651

Dañobeitia JJ, Canales JP (2000) Magmatic underplating in the Canary Archipelago. J Volcanol Geotherm Res 103:27–41

Day SJ, Carracedo JC, Guillou H, Gravestock P (1999) Recent structural evolution of the Cumbre Vieja volcano, La Palma, Canary Islands: volcanic rift zone reconfiguration as a precursor to volcano flank instability? J Volcanol Geotherm Res 94(1):135–167

Day SJ, Carracedo JC, Guillou H, Pais Pais FJ, Rodriguez Badiola E (2000) Comparison and cross-checking of historical, archaeological and geological evidence for the location and type of historical and sub-historical eruptions of multiple-vent oceanic island volcanoes. Geol Soc Lond Special Publ 171:281–306

Duggen S, Hoernle KA, Hauff F, Kluegel A, Bouabdellah M, Thirlwall MF (2009) Flow of Canary mantle plume material through a subcontinental lithospheric corridor beneath Africa to the Mediterranean. Geology 37(3):283–286

Fernández Santín S, Hernán Requera F, Navarro Falcones LF, Pliego Dones D (1974) Petrographic study of basaltic materials emitted by Teneguía volcano (La Palma, Canary Islands, October 27th–November 19th, 1971). Estud Geol. (Madrid) Teneguia. 27–34

Frost BR (1991) Introduction to oxygen fugacity and its petrological importance. In: Lindsley DH (ed) Oxide minerals: petrologic and magnetic significance. Mineralogical Society of America, Michigan. Reviews in Mineralogy 25:1–9. ISBN 0-939950-30-8

Galipp K, Klügel A, Hansteen TH (2006) Changing depths of magma fractionation and stagnation during the evolution of an oceanic island volcano: La Palma (Canary Islands). J Volcanol Geotherm Res 155:285–306

Hernández-Pacheco A, Valls MC (1982) The historic eruptions of La Palma Island (Canarias). Arquipelago Rev Univ Azores Ser C Nat 3:83–94

Herzberg C, Asimow PD (2008) Petrology of some oceanic island basalts: PRIMELTS2.XLS software for primary magma calculation. Geochemistry. Geophysics 9:Q09011. doi:10.1029/2008GC002057

Ibarrola E (1974) Temporal modification of the basaltic materials from 1971 eruption of the Teneguía volcano (La Palma, Canary Islands). Estud Geol (Madrid) Teneguia. 49–58

Klügel A (1998) Reactions between mantle xenoliths and host magma beneath La Palma (Canary Islands): constraints on magma ascent rates and crustal reservoirs. Contrib Mineral Petrol 131:237–257

Klügel A, Hansteen TH, Schmincke HU (1997) Rates of magma ascent and depths of magma reservoirs beneath La Palma (Canary Islands). Terra Nova 9(3):117–121

Klügel A, Schmincke HU, White JDL, Hoernle KA (1999) Chronology and volcanology of the 1949 multi-vent rift- zone eruption on La Palma (Canary Islands). J Volcanol Geotherm Res 94:267–282

Klügel A, Hoernle KA, Schmincke HU, White JDL (2000) The chemically zoned 1949 eruption on La Palma (Canary Islands): petrologic evolution and magma supply dynamics of a rift- zone eruption. J Geophys Res 105(B3):5997–6016

Klügel A, Galipp K, Hansteen TH (2005) Magma storage and underplating beneath Cumbre Vieja volcano, La Palma (Canary Islands). Earth Planet Sci Lett 236:211–226

Kovalenko VI, Naumov VB, Girnis AV, Dorofeeva VA, Yarmolyuk VV (2007) Volatiles in basaltic magmas of ocean islands and their mantle sources: I. Melt compositions deduced from melt inclusions and glasses in the rocks. Geochem Int 45(2):105–122

Kushiro I (1962) Clinopyroxene solid solutions. Part 1. The $CaAl_2SiO_6$ component. Jpn J Geol Geogr 13:213–229

Le Bas MJ, Streckeisen AL (1991) The IUGS systematics of igneous rocks. J Geol Soc Lond 148:825–833

Le Maitre RW, Streckeisen A, Zanettin B, Le Bas MJ, Bonin B, Bateman P, Bellieni G, Dudek A, Efremova A, Keller J, Woolley AR (2002) Igneous rocks. A classification and glossary of terms, Recommendations of the IUGS subcomission on the systematics of igneous rocks

Leake BE, Woolley AR, Arps CES, Birch WD, Gilbert MC, Grice JD, Hawthorne FC, Kato A, Kisch HJ, Krivovichev VG, Linthout K, Laird J, Mandarino JA, Maresch WV, Nickel EH, Rock NMS, Schumacher JC, Smith DC, Stephenson NCN, Ungaretti L, Whittaker EJW, Youzhi G (1997) Nomenclatures of amphiboles: report of the subcommittee on amphiboles of the international mineralogical association, commission on new minerals and mineral names. Can Mineral 35:219–246

Lepage LD (2003) ILMAT: an excel worksheet for ilmenite–magnetite geothermometry and geobarometry. Comput Geosci 29:673–678

Lindsley DH (1983) Pyroxene thermometry. Am Miner 68:477–493

Lindsley DH, Spencer KJ (1982) Fe-Ti oxide geothermometry: reducing analyses of coexisting Ti-magnetite (Mt) and ilmenite (Ilm). Eos Trans Am Geophys Union 63:471

Longpré MA, Troll VR, Hansteen TH (2008) Upper mantle magma storage and transport under a Canarian shield-volcano, Teno, Tenerife (Spain). J Geophys Res Solid Earth 113:B08203. doi:10.1029/2007JB005422

Lopez Ruiz J (1973) The pyroxenes of the alkali series rocks: the case of the pyroxenes of the Teneguia Volcano, La Palma, Canary Islands. Bol Geol Minero 84:56–60

Masotta M, Mollo S, Freda C, Gaeta M, Moore G (2013) Clinopyroxene—liquid thermometers and barometers specific to alkaline differentiated magmas. Contrib Mineral Petrol 166:1545–1561. doi:10.1007/s00410-013-0927-9

Miller MS, O'Driscoll LJ, Butcher AJ, Thomas C (2015) Imaging Canary Island hotspot material beneath the lithosphere of Morocco and southern Spain. Earth Planet Sci Lett 431:186–194

Mordick BE, Glazner AF (2006) Clinopyroxene thermobarometry of basalts from the Coso and Big Pine volcanic fields, California. Contrib Mineral Petrol 152:111–124

Muñoz M, Sagredo J, Afonso A (1974) Mafic and ultramafic inclusions in the eruption of Teneguisa volcano (La Palma, Canary Islands). Estud Geol (Madrid) Teneguia. 65–74

Neumann ER, Soerensen VB, Simonsen SL, Johnsen K (2000) Gabbroic xenoliths from La Palma, Tenerife and Lanzarote, Canary Islands: evidence for reactions between mafic alkaline Canary Island melts and old oceanic crust. J Volcanol Geotherm Res 103:313–342

Nikogosian IK, Elliott T, Touret JLR (2002) Melt evolution beneath thick lithosphere: a magmatic inclusion study of La Palma, Canary Islands. Chem Geol 183:169–193

Prægel N (1986) The petrology and geochemistry of Volcan Teneguía, La Palma, Canary Islands. Inst Petrol Cph Univ, Copenhagen

Praegel NO, Holm PM (2006) Lithospheric contributions to high-MgO basanites from the Cumbre Vieja Volcano, La Palma, Canary Islands and evidence for temporal variation in plume influence. J Volcanol Geotherm Res 149:213–239

Putirka K (1997) Magma transport at Hawaii: inferences based on igneous thermobarometry. Geology 25:69–72

Putirka K (1999) Clinopyroxene + liquid equilibria to 100 kbar and 2450 K. Contrib Mineral Petrol 135:151–163

Putirka K (2008) Thermometers and barometers for volcanic systems. Rev Miner Geochem 69:61–120

Putirka K, Johnson M, Kinzler R, Longhi J, Walker D (1996) Thermobarometry of mafic igneous rocks based on clinopyroxene-liquid equilibria, 0–30 kbar. Contrib Mineral Petrol 123:92–108

Putirka K, Mikaelian H, Ryerson FJ, Shaw H (2003) New clinopyroxene-liquid thermobarometers for mafic, evolved and volatile-bearing lava compositions, with applications to lavas from Tibet and the Snake River Plain, ID. Am Mineral 88:1542–1554

Ranero CR, Torne M, Banda E (1995) Gravity and multichannel seismic reflection constraints on the lithospheric structure of the Canary swell. Mar Geophys Res 17:519–534

Ridolfi F, Renzulli A (2012) Calcic amphiboles in calc-alkaline and alkaline magmas: thermobarometric and chemometric empirical equations valid up to 1,130°C and 2.2 GPa. Contrib Mineral Petrol 163:877–895. doi:10.1007/s00410-011-0704-6

Staudigel H, Feraud G, Giannerini G (1986) The history of intrusive activity on the island of La Palma (Canary Islands). J Volcanol Geotherm Res 27(3):299–322

Sterner SM, Bodnar RJ (1989) Synthetic fluid inclusions: VII. Reequilibration of fluid inclusions in quartz during laboratory simulated metamorphic burial and uplift. J Metamorph Geol 7:243–260

Stroncik NA, Klügel A, Hansteen TH (2009) The magmatic plumbing system beneath El Hierro (Canary Islands): constraints from phenocrysts and naturally quenched basaltic glasses in submarine rocks. Contrib Mineral Petrol 157(5):593–607

Sun S-S, McDonough WF (1989) Chemical and isotopic systematics of oceanic basalts: implications for mantle composition and processes. In: Saunders, AD, Norry MJ (eds) Magmatism in the ocean basins, vol 42. Geological Society Special Publication, London, pp 313–345

Tenzer R, Bagherbandi M, Vajda P (2013) Global model of the upper mantle lateral density structure based on combining seismic and isostatic models. Geosci J 17:65–73

Troll VR, Klügel A, Longpré MA, Burchardt S, Deegan FM, Carracedo JC, Wiesmaier S, Kueppers U, Dahren B, Blythe LS, Hansteen T, Freda C, Budd DA, Jolis EM, Jonsson E, Meade F, Berg S, Mancini L, Polacci M (2012) Floating sandstones off El Hierro (Canary Islands, Spain): the peculiar case of the October 2011 eruption. Solid Earth Discuss 3:975–999. doi:10.5194/sed-3-975-2011

Van Der Kerkoff AM, Hein UF (2000) Fluid inclusion petrography. Lithos 55:27–47

Vityk MO, Bodnar RJ (1995) Textural evolution of synthetic fluid inclusions in quartz during reequilibration, with applications to tectonic reconstruction. Contrib Mineral Petrol 121:309–323

Wallace PJ (2005) Volatiles in subduction zone magmas: concentrations and fluxes based on melt inclusion and volcanic gas data. J Volcanol Geotherm Res 140:217–240

Weis FA, Skogby H, Troll VR, Deegan FM, Dahren B (2015) Magmatic water contents determined through clinopyroxene; examples from the Western Canary Islands. Geochem Geophys Geosyst, Spain. doi:10.1002/2015GC005800